

**Review of Aeronautical Fatigue  
Investigations in Germany during the Period  
April 2013 to April 2015**

---

Dr. Claudio Dalle Donne and Michael Jürgens  
Airbus Group Innovations  
TX2

Title

Review of Aeronautical Fatigue Investigations in Germany during the Period  
April 2013 to April 2015

Author

Dr. Claudio Dalle Donne and Michael Jürgens

Phone

+49-89.607 27728

Department/Work area

TX2

Date

April 2015

Project-No.

Abstract

This review embodies a compilation of abstracts on aeronautical fatigue investigations in Germany during the period April 2013 to March 2013 and is presented within the scope of the Meeting of the International Committee on Aeronautical Fatigue in Helsinki, Finland, June 1st-5th 2015.

The contribution of summaries by German aerospace manufacturers, governmental and private research institutes, universities as well as aerospace authorities was completely voluntary, and is acknowledged with sincere appreciation by the authors of this review.

Enquiries concerning the contents should be addressed directly to the author of the corresponding summary.

Distribution to

Bilfinger-HSG – digitale Bibliothek (e-mail or DVD to Mrs. Fleißner)

pages

39

Keywords for database

International Committee on Aeronautical Fatigue, ICAF 2015, National Delegate Review

**1** Classification

- 1 generally accessible
- 2 free distribution inside Airbus Group
- 3 confidential
- 4 highly confidential

Acceptance

**Dr. Claudio Dalle Donne**

Team-/Department Leader  
(Approve Document)

**Dr. Claudio Dalle Donne**

HoTCC/Local Representative  
(Validate Document)

## Table of contents

1	Introduction.....	6
2	Full Scale Testing.....	7
2.1	Airbus A350 XWB – Full Scale Fatigue Test EF2.....	7
2.2	Airbus A350 XWB – Full Scale Static and Fatigue Test EW.....	8
2.3	Airbus A400M – Full Scale Fatigue Test.....	10
2.4	Door Structure Testing.....	12
2.5	Engine Structure Testing.....	13
3	Fatigue and Fracture of Fuselage Panels and Joints.....	14
3.1	Curved Panel Testing.....	14
3.2	Crack propagation resistance of metallic z-reinforced CFRP joints.....	15
3.3	Retardation of fatigue crack growth in thin AA2024 sheets by laser heating.....	16
3.4	Innovative manufacturing and joining concepts for load-bearing titanium-CFRP structures.....	18
3.5	Tensile strength and fatigue properties of laser beam welded Ti-6Al-4V sheets subjected to superplastic forming.....	20
3.6	Biaxial fatigue testing of crenellated fuselage panels.....	22
4	Fatigue Life Assessment and Prediction.....	24
4.1	Fracture mechanical investigations of defects and surface roughness on the fatigue performance of additive manufactured Ti-6Al-4V.....	24
5	Fatigue and Fracture of Metallic Fuselage Materials.....	25
5.1	Enhancement of the fatigue properties of the metastable $\beta$ titanium alloy Ti 38-644 by obtaining a superior microstructure via Thermohydrogen Treatment (THT).....	25
5.2	Hydride-induced improvement of fatigue properties of the high-strength $\beta$ titanium alloy Ti 10-2-3 by Thermohydrogen Treatment (THT).....	27
5.3	Laser Shock Peening as Surface Technology to extend Fatigue Life in Metallic Airframe Structures.....	29
6	Fatigue and Fracture of Engine Materials.....	32
6.1	High-temperature low cycle and thermomechanical fatigue behaviour of titanium aluminides.....	32
6.2	Influence of fatigue frequency and hold-time on the crack propagation in IN718 in the temperature range of dynamic embrittlement.....	33
6.3	High temperature low cycle fatigue testing technique for miniature specimens from single crystal super alloys for gas turbine blades.....	35
6.4	Hydrogen embrittlement of pulse-plated nickel.....	37

## Tables

Table 7-1: Percentage of measured intercrystalline fracture for crack propagation test at 650°C at a stress ratio of $R = 0.1$ in laboratory air for two sinusoidal load modes at frequencies of 1 Hz and 4 Hz and a dwell times test with a dwell time of 3 s and load ramps of 2 s.....	35
---	----

## Figures

Figure 2-1: Road transport of A350 XWB EF2 centre fuselage.....	7
Figure 2-2: A350 XWB EF2 test set up at IABG .....	8
Figure 2-3: Ultimate load up bend test at the A350 XWB EW test at IABG .....	9
Figure 2-4: A400M FSFT test set up at IABG .....	11
Figure 2-4: Door structure test at IMA.....	12
Figure 2-4: IMA engine test set-up.....	13
Figure 2-4: Curved panel test facility at IMA. ....	14
Figure 3-1: a) Aimed application of through-thickness reinforcements and b) Layup of reinforced DCB specimens – (1) laminate, (2) reinforcement sheet, (3) adhesive and Teflon foil, (4) laminate, (5) sheet for stiffness compensation .....	15
Figure 3-2: Critical SERR vs. crack propagation and approximated R-curve of metallic z-reinforced CFRP joints compared to a co-bonded reference.....	16
Figure 3-3: Sketch of the investigated M(T)200 specimen. Marked in green, blue and red are the laser heating lines, (a) with two heating lines, (b) with four, and (c) with six heating lines correspondingly. ....	17
Figure 3-4: Fatigue crack growth behaviour of M(T)200 specimens at R-ratio 0.1, laser heated specimens compared to the base material.....	18
Figure 3-5: Fatigue crack growth rate vs. the number of applied load cycles of the laser heated M(T)200 specimens at R-ratio 0.1 compared to the base material. ....	18
Figure 3-6: Door surrounding prototype component [3].....	19
Figure 3-7: (a) Results of lap-shear fracture testing and (b) macrograph of a laser-riveted specimen with 11 x 2.0-mm pins and 2 x 4.8-mm pins; cross section of a 4.8-mm diameter laser rivet.....	19
Figure 3-8: (a) Stress-strain curves of tested Ti-6Al-4V FG and STD BMs and dissimilar laser beam welded FG-STD butt joint; (b) FCP test results. ....	21
Figure 3-9: Deformed specimens from the cone-cup test (a) at 0.92 MPa and (b) 1.09 MPa. ....	21
Figure 3-10: (a) the triaxial testing facility, (b) a detailed view of the experimental set-up and (c) the corresponding FEM model. ....	23
Figure 3-11: (a) comparison of fatigue crack propagation rate under uniaxial (biaxial load ratio: $\chi=0$ ) and biaxial ( $\chi=0.5$ ) loading conditions, (b) fatigue life improvement of crenellated panels compare to flat panels under uniaxial and biaxial loading conditions .....	23
Figure 4-1: left: typical surface roughness for DMLS, right: typical defects for EBM .....	24
Figure 5-1: ) $T_{\beta}$ as function of the hydrogen content; HADA-THT strategy of $\beta$ -C is marked schematically by ABCDEF; b) microstructure finally obtained after 5-step HADA-THT; c) reference microstructure after duplex-aging cycle.....	26
Figure 5-2: Results of the staircase test applied to the 5-step HADA-THT treated $\beta$ -C a) sequence of tests, b) statistical evaluation .....	26
Figure 5-3: a) HIRB-THT strategy inscribed schematically by ABCDEF in the $T_{\beta}$ diagram; FE-SEM micrographs after THT-steps b) hydrogenation (BC) and c) recrystallization (CD) ...	28
Figure 5-4: Results of the staircase test applied to a) conventional technical heat treatment as reference condition and b) 5-step HIRB-THT treated material (sequence of tests) .....	28
Figure 5-5: Example of through thickness compressive residual stress in Al alloys up to 6mm thickness laser shock peened, from both sides (left) and crack growth behavior (da/dN vs. DK curve) in Al2024-T351 after LSP treatment (right).....	30
Figure 5-6: Through the thickness residual stress profile (left) and crack growth curve under constant amplitude loading (R=0.1) in Al7010-T7451 30mm thick plate.....	31
Figure 5-7: Crack propagation curves determined under spectrum loading in as machined and laser shock peened condition. ....	31

Figure 7-1: Suitable agreement between simulated and obtained TMF hysteresis loop at the beginning (a) of the test as well as at the half (b) of the fatigue life ( $N_f/2$ )..... 32

Figure 7-2: Comparison between the obtained and the calculated fatigue life under TMF and LCF conditions..... 33

Figure 7-3: Crack propagation rates at 650°C with a load ratio of  $R = 0.1$  tested in air and vacuum. The load was either applied sinusoidal at 1 Hz and 4 Hz or in a dwell-time test with dwell-times of 3 s, 26 s, 96 s and 296 s and load ramps of 2 s. .... 34

Figure 7-3: Miniature specimen for high temperature fatigue tests (a) macro photograph and (b) stress distribution for specimens with length axis in different crystallographic orientations under tensile load (stress component  $S_{22}$  in loading direction shown)..... 36

Figure 7-3: Cross sections of specimen after LCF at 950°C. (a) Overview of pore chains aligned along solidification dendrites. (b) Multiple crack growth at internal pores. (c) Deformation band at crack tip along  $\langle 111 \rangle$  plane of the single crystal,  $\gamma'$ -precipitates were sheared and small intermetallic precipitates (see arrows) occurred..... 36

## 1 Introduction

This review embodies a compilation of abstracts on aeronautical fatigue investigations in Germany during the period April 2013 to March 2015 and is presented within the scope of the Meeting of the International Committee on Aeronautical Fatigue in Helsinki, Finland, June 1st-5th 2015.

The contribution of summaries by German aerospace manufacturers, governmental and private research institutes, universities as well as aerospace authorities was completely voluntary, and is acknowledged with sincere appreciation by the authors of this review.

Enquiries concerning the contents should be addressed directly to the author of the corresponding summary.

### Mailing addresses of contributing companies and institutes:

Abbreviation	Details
AD	Airbus Defence and Space, Airbus DS GmbH, Robert-Koch-Straße 1, D-82024 Munich, Germany, <a href="http://www.airbusdefenceandspace.com">www.airbusdefenceandspace.com</a>
AGI	Airbus Group Innovations, D-81663 Munich, Germany, <a href="http://www.airbusgroup.com">www.airbusgroup.com</a>
Airbus	Airbus Operations GmbH; Kreetslag 10, D-21129 Hamburg, Germany, <a href="http://www.airbus.com">www.airbus.com</a>
DLR	German Aerospace Centre, Institute of Materials Research, 51147 Cologne Germany, <a href="http://www.dlr.de">www.dlr.de</a>
FT	FormTech GmbH, Mittelwendung 26, 28844 Weyhe, Germany <a href="http://www.formtech.de">www.formtech.de</a>
HZG	Helmholtz-Zentrum Geesthacht; Max-Planck-Straße 1, D-21502 Geesthacht, Germany, <a href="http://www.hzg.de">www.hzg.de</a>
IABG	Industrieanlagen-Betriebsgesellschaft mbH; PO-Box 1212, D-85503 Ottobrunn, Germany, <a href="http://www.iabg.de">www.iabg.de</a>
IMA	IMA Materialforschung und Anwendungstechnik GmbH; Postfach 80 01 44, D-01101 Dresden, Germany, <a href="http://www.ima-dresden.de">www.ima-dresden.de</a>
LMW	University of Siegen, Research Group for Material Science and Material Testing; Paul-Bonatz-Strasse 9-11, D-57076 Siegen, Germany, <a href="http://www.uni-siegen.de">www.uni-siegen.de</a>

## 2 Full Scale Testing

### 2.1 Airbus A350 XWB – Full Scale Fatigue Test EF2

*F. Schorr (IABG)*

With the delivery of the main specimen sections (fuselage centre section and both wings) in June 2013 the on-site activities for the A350 XWB EF2 (Essay Fatigue) full scale fatigue test started at IABG's test hall in Erding. The specimen sections were delivered to Munich Airport by Airbus A300ST Beluga airplanes and transported to IABG by road transport (see Figure 2-1).

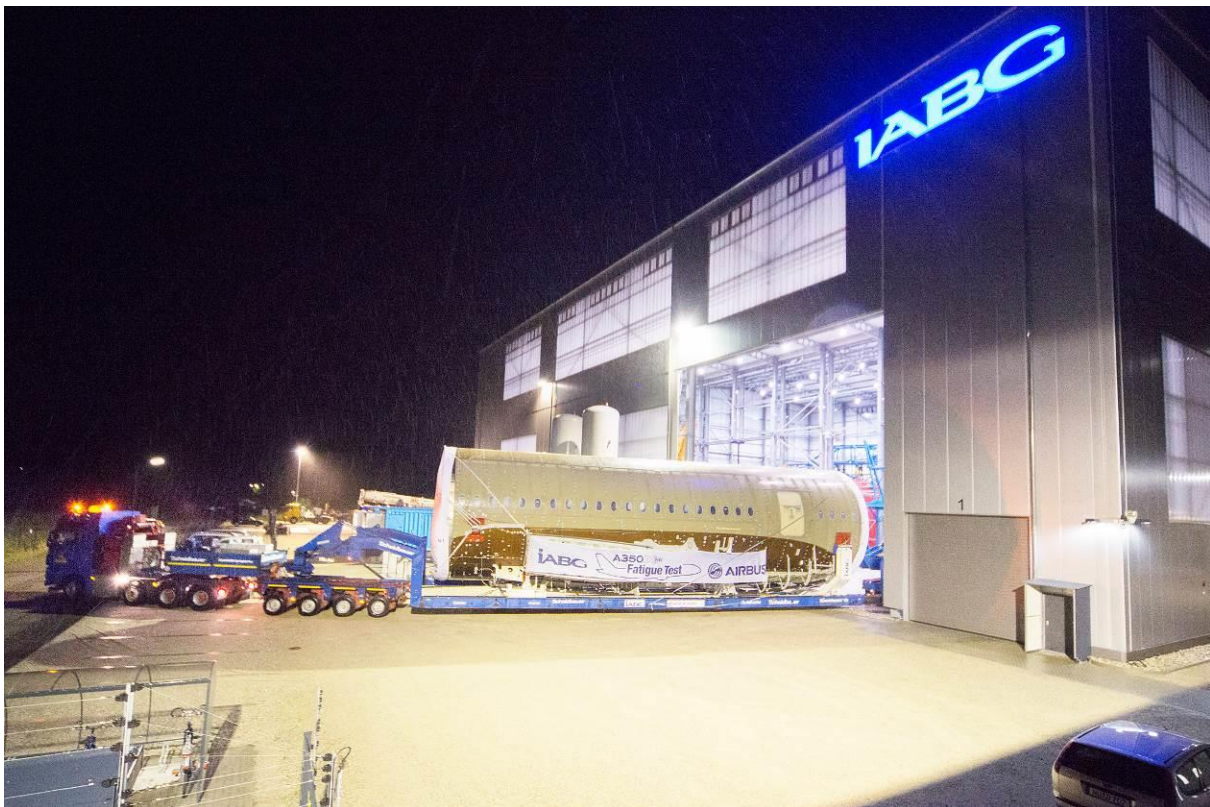


**Figure 2-1: Road transport of A350 XWB EF2 centre fuselage**

The EF2 test specimen includes the primary structure of the fuselage centre section incl. doors and the both wings, major components of the main landing gears and the belly fairing. It is loaded by 88 servo-hydraulic actuators which are connected to the specimen via whiffle trees, dummy structures, load fittings and bulkheads. The steel bulkheads are attached to the specimen at the forward and aft end of the centre fuselage to introduce interface forces resulting from the nose and rear fuselage sections and to make the centre fuselage air tight for pressurization during each simulated flight. The whole specimen is supported on 6 restraint rods. The data acquisition system is able to measure and record strains, deflections and loads from more than 4,000 measurement channels with a measurement rate of 100Hz.

The main focus of the EF2 test is to demonstrate and validate the fatigue behavior of the metallic structure of the specimen in combination with the reinforced plastics. Therefore up to 3 De-

sign Service Goals (DSG) of flight cycles will be simulated followed by a residual strength campaign.

The final assembly of the specimen and the installation of the test set up were completed by the end of 2013 (see Figure 2-2) followed by the commissioning of the overall test by May 2014. Afterwards the fatigue testing started: 24 hours per day and 7 days a week operations including inspections, performed by IABG inspection staff.

With the simulation of more than 3,850 flights at the beginning of July 2014 IABG was able to support the customer Airbus with the mandatory input needed for the certification of the A350 XWB which was successfully granted by EASA in September 2014.

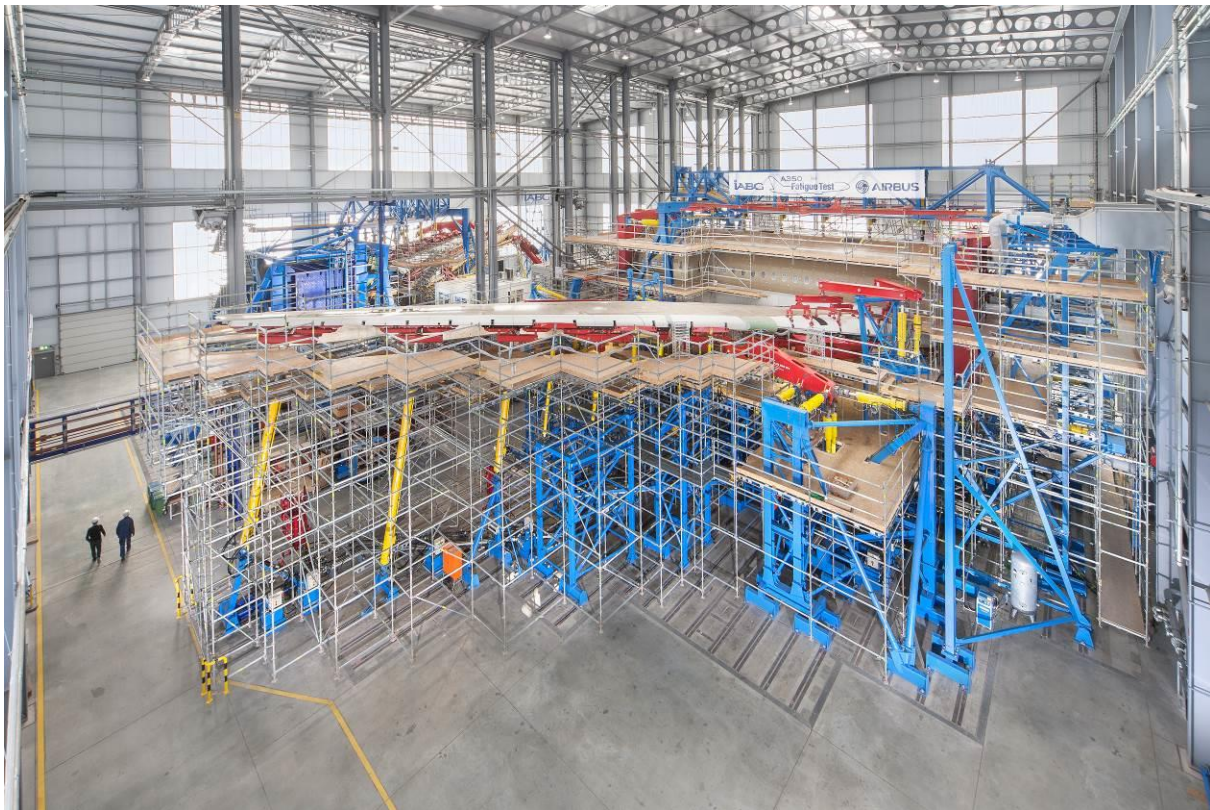


**Figure 2-2: A350 XWB EF2 test set up at IABG**

## **2.2 Airbus A350 XWB – Full Scale Static and Fatigue Test EW**

*F. Schorr (IABG)*

In August 2014 IABG successfully completed the A350 XWB EW (Essay Wing) full scale test including several first flight and certification relevant test campaigns.

Within the full scale test EW the left hand wing structure of the Airbus A350 XWB was tested. Main focus of the static, dynamic and functional tests was the validation and certification of the material behavior of CFRP in conjunction with metallic materials. The aim of the test was to prove static and fatigue behavior as well as damage tolerance of the primary structure of the wing which is made of more than 50% reinforced plastics (mainly CFRP). Up to 41 servo-

hydraulic actuators loaded the specimen via individual whiffle trees, load introduction fittings and dummy structures. During the individual test campaigns up to 3,000 measurement channels recorded strains and deflections of the wing structure. The test results were fundamental requirements for the certification of the Airbus A350 XWB.

First functional and static tests were already performed in 2013 by IABG and corresponding test results were delivered in time to the customer Airbus to enable first flight clearance for the A350 XWB in June 2013.

Between January and March 2014 the fatigue test up to 1 Design Service Goal (DSG) of simulated flights was performed with 24/7 shift operation. As part of the fatigue test IABG performed regular inspections of the specimen structure. The certification relevant test plan also included static campaigns of the wing structure up to ultimate load. The ultimate load campaign was performed during April 2014 including the ultimate load up bend test (see Figure 2-3). By June 2014 the performance of another 0.5 DSG of simulated flights was successfully completed. The last test campaign included static tests up to limit load.

After test completion in August 2014 IABG started the dismantling of the specimen and the surrounding test set up and was able to deliver the cut specimen sections back to Airbus by November 2014.



**Figure 2-3: Ultimate load up bend test at the A350 XWB EW test at IABG**

## **2.3 Airbus A400M – Full Scale Fatigue Test**

*F. Schorr, O. Tusch (IABG)*

From 2011 to 2014 IABG successfully performed the full scale fatigue test of the Airbus A400M incl. performance of 2.5 design service goals and residual strength tests.

The full scale fatigue test specimen (see Figure 2-4) of the military transporter Airbus A400M included mainly the primary structure of the pressurized fuselage incl. cargo ramp and cargo door and the wings incl. wing to fuselage fairing. Main parts of a serial aircraft like the 6 axes landing gears and the engines were replaced by corresponding dummy structures or interface fittings on the primary structure were directly loaded by servo-hydraulic actuators. All in all the fatigue specimen was loaded by 97 servo-hydraulic actuators connected to the specimen via whiffle trees, dummy structures or load introduction fittings and additionally several serial aircraft hydraulic actuators for cargo ramp operations. The specimen was bedded on 6 restraint rods. A data acquisition system with the capability to measure and record more than 4,000 measurement channels was installed.

The aim of the A400M full scale fatigue test was to demonstrate and proof the fatigue and damage tolerance behaviour of the metallic structure of the aircraft. The A400M as a military transport aircraft has special requirements regarding airdrop functionality. Therefore the cargo ramp and cargo door were also operated during simulation of flights in the fatigue test.

IABG performed fatigue testing of 2.5 design service goals on the basis of a military mission mix incl. introduction of artificial damages, static & regular SHM like measurement campaigns and inspections between 2011 and 2013. The fatigue test was performed with a test speed of more than 1,100 flights per week which was only possible due to special IABG designed theoretical control models supported by FE models of the specimen by the customer. These special control models allow very high test speed combined with fulfilment of customer's high test accuracy requirements.

Up to June 2014 the residual strength tests including artificial damages tests were successfully performed. The results of the A400M full scale fatigue test were a major input for EASA type certification.

After test completion in June 2014 IABG started the dismantling of the specimen and the surrounding test set up and was able to deliver the cut specimen sections back to Airbus by November 2014.



**Figure 2-4: A400M FSFT test set up at IABG**

## 2.4 Door Structure Testing

*S. Nebel (IMA)*

Within a research project a CFRP aircraft door was tested under static and fatigue load cases. For this purpose a special designed test rig, including a dummy fuselage structure with representative stiffness and capability to apply internal pressure, was developed.

Overall dimensions of the set-up were 2 x 3 x 4 m. The pressure chamber of the set-up was able to provide over pressure up to 2 bar. 12 hydraulic actuators at the door interfaces were used to simulate barrel deformations under internal pressure.

During the tests door deformations and strains were measured using strain gauges and the digital stereo image correlation system ARAMIS. To proof structural integrity with damages, impacts and saw cuts were implemented in different structural elements of the door. Propagation of artificial damages was investigated with ultrasonic NDI-methods during the tests.

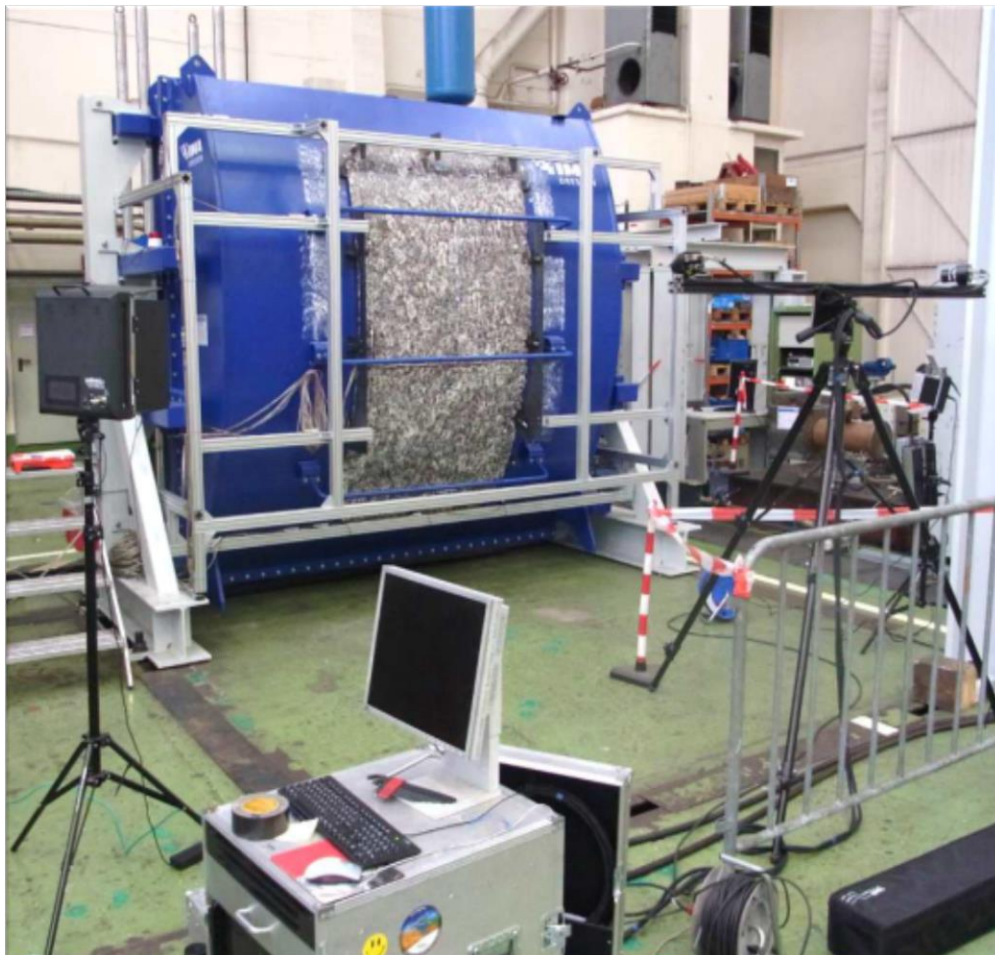


**Figure 2-5: Door structure test at IMA.**

## 2.5 Engine Structure Testing

*S. Nebel (IMA)*

A fatigue test at the Trent XWB ICC was performed by IMA Dresden in 2014. In order to load the component properly, dummy structures replacing fan case and combustor chamber outer case were used.

In total, 20 hydraulic actuators were used to load the specimen at different flanges and at bearing supports. 3 design service goals for the intact specimen were performed. The instrumentation consisted of 30 strain gauge channels and 46 displacement sensors.

Fatigue cycling for a failsafe condition of the engine mounts and crack propagation testing with artificial defects will be performed in the near future.

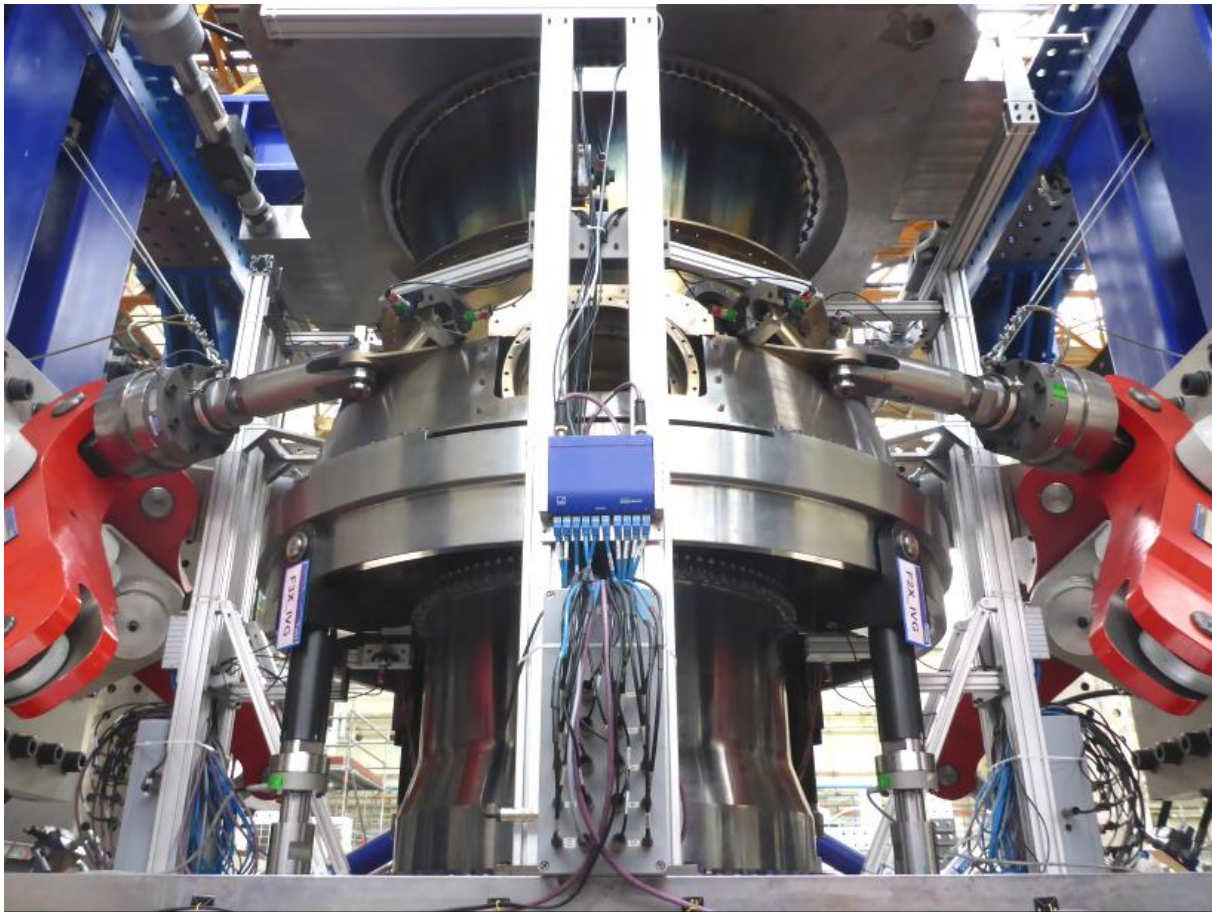


**Figure 2-6: IMA engine test set-up.**

### 3 Fatigue and Fracture of Fuselage Panels and Joints

#### 3.1 Curved Panel Testing

*S. Nebel (IMA)*

For the development of the A350XWB-1000 a curved panel test of an upper shell of the fuselage was performed at IMA Dresden's test rig V4.

The panel was loaded statically with the following load components:

- Overpressure
- Axial load, tension and compression
- Constant in-plane shear
- Lateral force to achieve distributed shear stresses

293 strain gauge channels were applied to monitor specimen behavior. The digital stereo image correlation system ARAMIS was used to gather information mainly regarding skin buckling behavior.

To proof structural integrity with damages, impacts with various energies were subsequently applied to different structural elements.



**Figure 3-1: Curved panel test facility at IMA.**

### 3.2 Crack propagation resistance of metallic z-reinforced CFRP joints

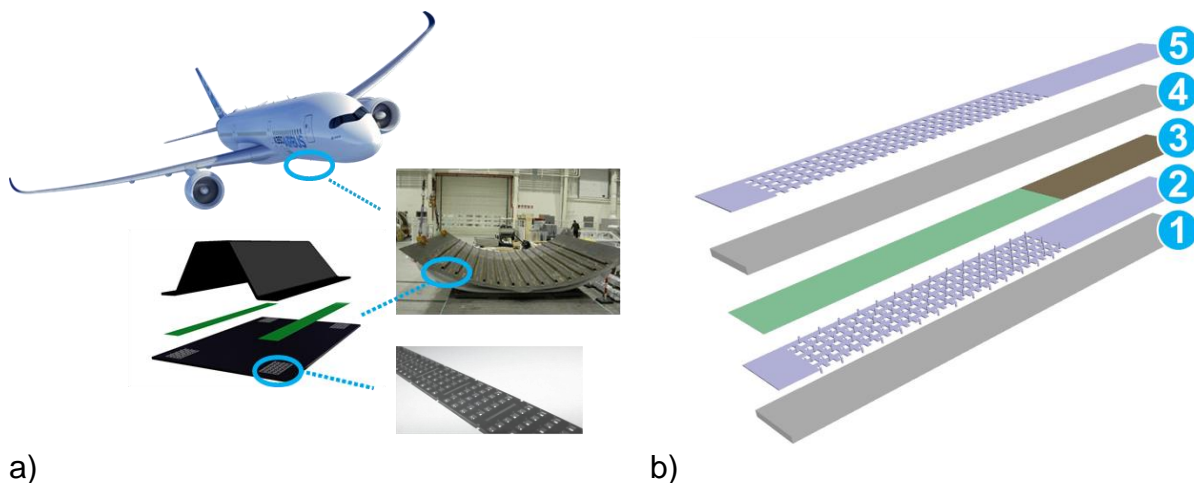
*M. Jürgens (AGI)*

Weight savings potential of carbon fiber reinforced polymers (CFRP) in primary aircraft structures is strongly determined by the applied joint design [1]. Reinforcements in through-thickness direction aim at efficiently transferring load between adherents and improving the level of joint damage tolerance [2]. An innovative reinforcement technology encompasses cost and time efficient manufacturing and crack arresting properties. Metallic sheets of e.g. titanium or stainless steel are consecutively stamped and bent and introduced into the joining area before curing the laminate [3].

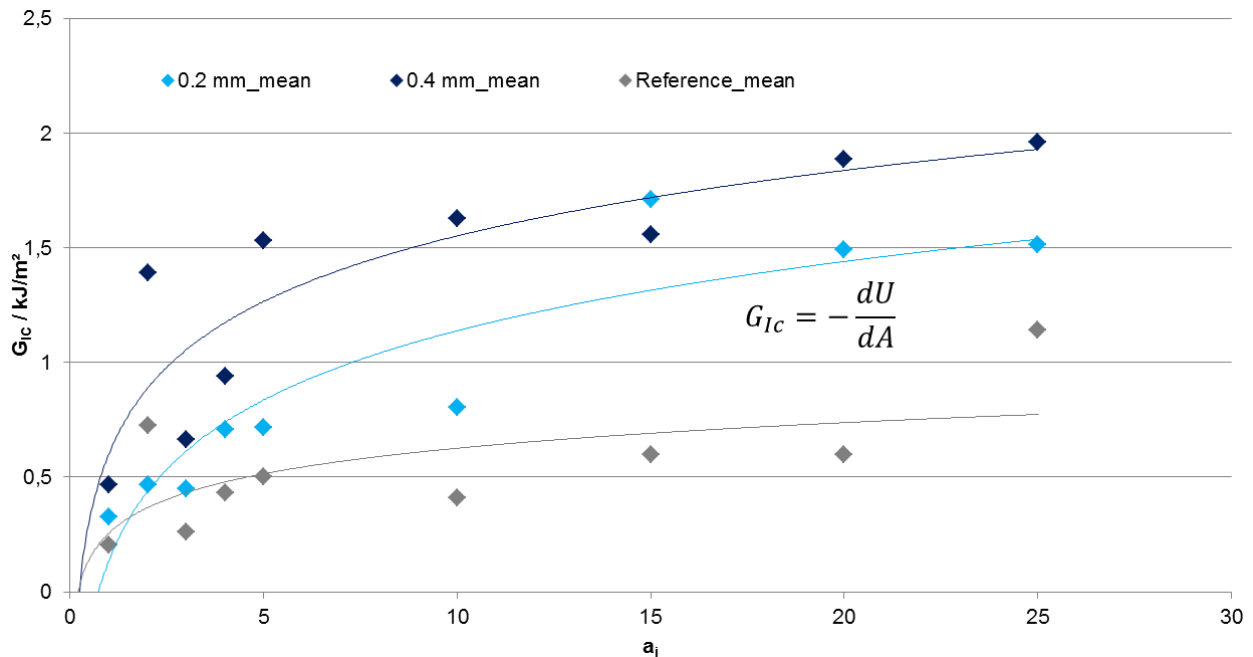
The impact of reinforcement thickness crack propagation behaviour of CFRP joints was determined on a double cantilever beam (DCB) geometry, using SAE 304 stainless steel as the reinforcement material and M21/T800S unidirectional prepreg to build up the CFRP adherents. FM300M .05 film adhesive was applied after the first co-bonding cycle to join the laminate.

Figure 3-3 depicts the critical strain energy release rate (SERR) versus crack propagation of z-reinforced CFRP joints.

$G_{IC}$  values were increased by more than 90 % for 0.4 mm thickness sheets compared to the co-bonded reference. An extending gap of SERR was observed with further crack propagation, which is related to the increasing amount of reinforcing spikes interacting with the laminate. Initial adhesive failure and traction during spike pull-out were revealed to be the two major energy absorbing mechanisms for the reinforced joints.



**Figure 3-2: a) Aimed application of through-thickness reinforcements and b) Layup of reinforced DCB specimens – (1) laminate, (2) reinforcement sheet, (3) adhesive and Teflon foil, (4) laminate, (5) sheet for stiffness compensation**



**Figure 3-3: Critical SERR vs. crack propagation and approximated R-curve of metallic z-reinforced CFRP joints compared to a co-bonded reference**

- [1] Kolesnikov, B., Herbeck, L., Fink, A. "CFRP/titanium hybrid material for improving composite bolted joints". *Composite Structures* 83(4) (2008): 368-380.
- [2] Mouritz, A. P. "Review of z-pinned composite laminates." *Composites* 38(12) (2007): 2383-2397.
- [3] Nogueira, A. C., Drechsler, K., Hombergsmeier, E. "Analysis of the Static and Fatigue Strength of a Damage Tolerant 3D-reinforced Joining Technology on Composite Single Lap Joints." 53rd AIAA/ASME/ASCE/AHS/ASC Structures, Structural Dynamics and Materials Conference. Honolulu, HI (US), 2012.

### 3.3 Retardation of fatigue crack growth in thin AA2024 sheets by laser heating

*A. Groth, M. Horstmann, N. Kashaev, and N. Huber (HZG)*

Welding processes have a potential to save weight and therefore costs in structural components. During production of these components thermal and mechanical processes introduce residual stresses. These residual stresses influence the fatigue lifetime [1]. As a possible method to improve the residual stress state of such components, local laser heating was applied by Schnubel et al. [2]. It was demonstrated in previous works, that laser heating is an appropriate method to retard fatigue crack growth [2-3]. Laser heating introduces tensile stresses in the centre of the heating line. The induced compressive stresses, compensating these tensile stresses in the base metal, are expected to significantly retard the fatigue crack growth before the crack reaches the position of the heating lines.

In order to investigate this effect the corresponding experiments were carried out on M(T)200 specimen with a thickness of 2 mm. A typical airplane aluminium alloy AA2024 T3 was used.

The laser heating lines were performed with a laser power of 600 W and a beam movement

velocity of 1.6 m/min. In order to prevent local melting on the specimen surface a defocussed laser beam was used. In this case the illuminated area was widened to a spot diameter of 3.5 mm.

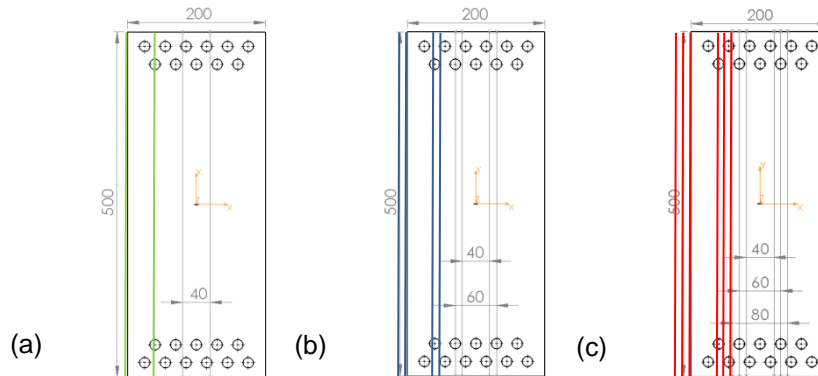


**Figure 3-4: Sketch of the investigated M(T)200 specimen. Marked in green, blue and red are the laser heating lines, (a) with two heating lines, (b) with four, and (c) with six heating lines correspondingly.**

Eventually, the effectiveness of the laser heating treatment to improve the damage tolerance behaviour was tested by constant stress amplitude fatigue crack growth tests (R-ratio 0.1 and frequency 5 Hz). Figure 3-5 shows the crack length vs. the applied load cycles for the differently treated samples. In case of the afore mentioned laser heating parameter set, two lines on each specimen increase the fatigue life by 10 % in comparison to the base material. This agrees nicely with former results where the effect of different laser parameter sets were compared [4].

In order to further increase the fatigue life, additional heating lines in a distance as shown in Figure 3-4 (b)-(c) were applied. A second and a third line in a distance of 10 mm was added on each side. With two lines on each side an increase of 20 % is reached in comparison to the base material. With three lines on each side a gain of approximately 70 % in load cycles before failure is reached. Interestingly, when the propagating crack reaches the area near a heating line, a sudden retardation of the crack growth can be observed. After passing the heating line area the crack growth rate reaches its former value again. This trend becomes less distinct if the number of heating lines increases.

The influence of the residual stresses on the crack growth rate can be directly observed in the corresponding curve represented by the fatigue crack growth rate vs. the number of applied load cycles, as shown in Figure 3-6. The positions of the heating lines are marked by dashed lines in the same colour and the achieved number of load cycles endured up to this crack length can be read from the abscissa. The increasing crack growth rate at these positions is clearly visible.

As an outlook for further increase in fatigue lifetime the whole design of laser heating patterns, i.e. line distance, line shapes and the number of lines can be optimised. Further investigations are work in progress.

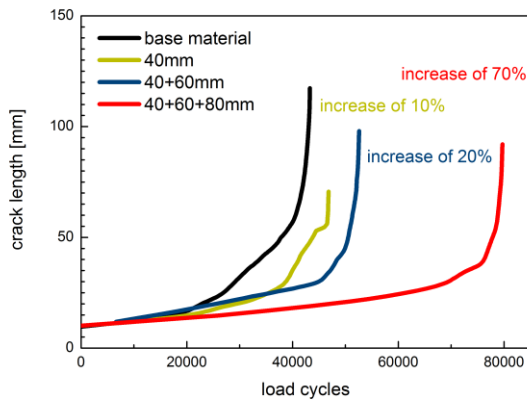


**Figure 3-5: Fatigue crack growth behaviour of M(T)200 specimens at R-ratio 0.1, laser heated specimens compared to the base material.**

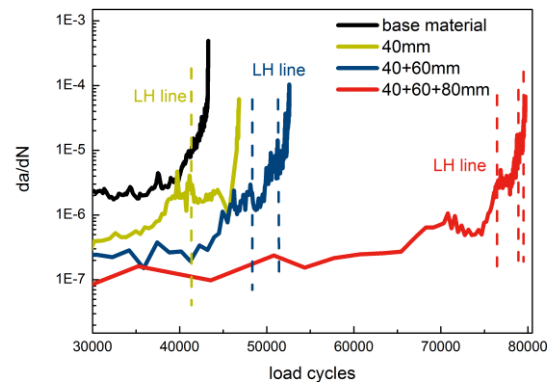


**Figure 3-6: Fatigue crack growth rate vs. the number of applied load cycles of the laser heated M(T)200 specimens at R-ratio 0.1 compared to the base material.**

- [1] Masubuchi, K. (1980), Analysis of welded structures: Residual stresses, distortion, and their consequences, Pergamon Press.
- [2] Schnubel, D., Horstmann, M., Ventzke, V., Riekehr, S., Staron, P., Fischer, T., Huber, N. (2012), Materials Science and Engineering A, vol. 546, pp. 8-14.
- [3] Schnubel, D. (2012), Laser heating as approach to retard fatigue crack growth in aircraft aluminium structures, PhD thesis, Hamburg University of Technology, Hamburg, Germany
- [4] Groth, A., Kashaev, N., Huber, N. (2014), In: Proceedings of the 29th Congress of the International Council of the Aeronautical Sciences, ICAS 2014, St. Petersburg, Russia, September 7-12.

### 3.4 Innovative manufacturing and joining concepts for load-bearing titanium-CFRP structures

*N. Kashaev, V. Ventzke, M. Horstmann, S. Riekehr (HZG) and W. Beck (FT)*

Titanium components are very expensive due to the lack of available cost-effective manufacturing processes. Machining as a conventional method to produce titanium components for the aerospace industry is characterised by low cutting speeds and tool lifetime. In case of milling, a high scrap rate as high as 95% is common. Within the frame of the OPTiSTRUCT project funded by the German Federal Ministry of Education and Research innovative joining concepts and manufacturing technologies for the realisation of titanium-CFRP structures were developed [1]. Instead of machining the cost-effective manufacturing and joining processes like hot deep drawing and laser beam welding (LBW) can be used for the realization of load-bearing titanium structures. In the present work the feasibility of hot deep drawing process for the production of a U-shaped prototype component similar to an aircraft door surrounding part under industrial conditions and requirements was examined (Figure 3-7) [2].

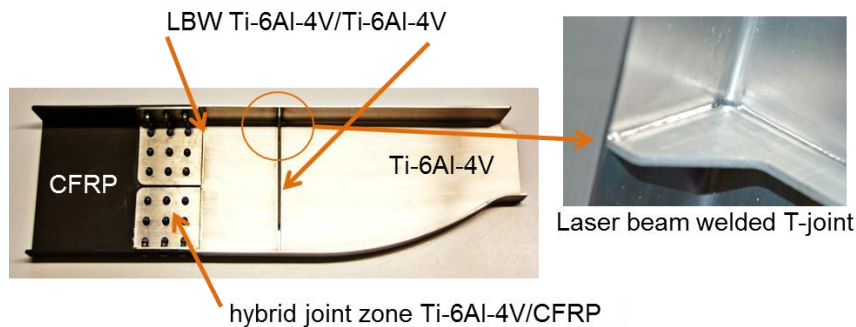
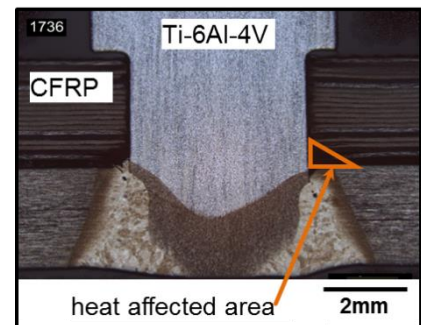
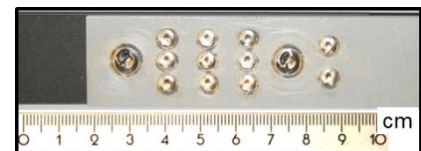
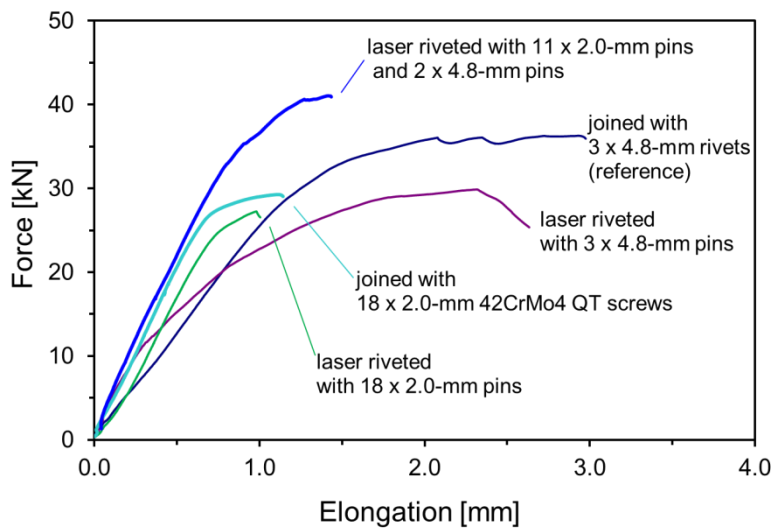


**Figure 3-7: Door surrounding prototype component [3].**



(a)

(b)

**Figure 3-8: (a) Results of lap-shear fracture testing and (b) macrograph of a laser-riveted specimen with 11 x 2.0-mm pins and 2 x 4.8-mm pins; cross section of a 4.8-mm diameter laser rivet.**

The current overlap joining method for CFRP and titanium is still based on classical riveting technology. In this work, the interface between CFRP and Ti-6Al-4V is characterised by a hybrid joint zone (Figure 1). Within the frame of the OPTiSTRUCT project, alternative joining methods to achieve improved strength and fatigue limit properties for the hybrid joint zone between CFRP and Ti-6Al-4V were developed [3]. One approach is using LBW as a joining technology [4]. LBW (denoted also as laser riveting of Ti-6Al-4V/CFRP lap joint) process was developed and optimized in terms of the temperature distribution to avoid thermal damage of CFRP structure, the interface properties and the mechanical structure of the hybrid joint zone (Figure 2(b)). The design of the laser riveted hybrid joint zone was developed using FEM simulations that examined pin positioning and size. Further approaches included the combination of an adhesive film, rivets and the use of a geometrically structured Ti-6Al-4V surface to obtain a reinforcing pinning effect. Both a classical riveted joint and the modified hybrid joint zones were tested in standard lap-shear fracture tests (Figure 3-8 (a)) and fatigue tests to understand and compare their properties and failure mechanisms. Hybrid joints produced by LBW exhibit a strength that is comparable to a classically riveted joint (Figure 2(a)).

In the final stages of the project, a Ti-6Al-4V/CFRP demonstrator representing an aircraft door surrounding prototype component was designed and realized (Figure 3-7). Feasibility studies were performed to examine the suitable process parameters needed to produce defect-free laser beam welded Ti-6Al-4V T-joints as well as to reduce both the weight and manufacturing costs.

- [1] Final Report to the project “Material and Cost Saving Production Processes for Titanium and New Design of the Joining Area CFRP-Ti as Hybrid Structure for Improvement of Load Transfer and Life Time / OPTISTRUCT”, funded by the German BMBF under contract no. 03CL05C within the Aviation Cluster Hamburg Metropolitan Region (2014), FormTech GmbH, Weyhe, Germany.
- [2] Stutz, L., Beck, W., Arends, S., Horstmann, M., Ventzke, V., Kashaev, N. (2014), *Materialwissenschaft und Werkstofftechnik*, vol. 40, n. 9, pp. 841-846.
- [3] Kashaev, N., Ventzke, V., Kolossa, S., Riekehr, S., Horstmann, M., Fomichev, V., Arends, S., Beck, W. (2014), In: *Proceedings of the Greener Aviation 2014 Conference, Clean Sky Breakthroughs and Worldwide Status*, Brussels, Belgium.
- [4] Kashaev, N., Ventzke, V., Riekehr, S., Horstmann, M. Under revision by Materials and Design.

### **3.5 Tensile strength and fatigue properties of laser beam welded Ti-6Al-4V sheets subjected to superplastic forming**

*N. Kashaev, V. Ventzke, M. Horstmann, S. Riekehr (HZG) and W. Beck (FT)*

High strength and sufficient ductility together with low density and high corrosion resistance are characteristic of the standard titanium alloy Ti-6Al-4V. The metallic components integrated in CFRP structures are therefore increasingly made with the alloy Ti-6Al-4V. A new fine grained Ti-6Al-4V sheet material variant has recently become available [1], which is characterized by high strength and reduced process temperatures and times in the superplastic forming (SPF) process. Therefore, cost-effective industrial manufacturing processes can be realised in conjunction with enhanced environmental performance. However, this material has not been approved for aerospace applications, and fine-grained Ti-6Al-4V sheets (denoted as FG) are more expensive than standard Ti-6Al-4V sheets (denoted as STD). Within the frame of the CoolTiTech project funded by the German Federal Ministry of Economics and Technology (BMWi) under the LuFo IV-3 program, it was investigated whether the superior properties of Ti-6Al-4V FG sheets may be dissimilarly combined with Ti-6Al-4V STD sheets to enhance the functionality and reduce the cost [2]-[3].

A Ti-6Al-4V FG sheet that has been developed for SPF processes at temperatures below 950 °C was successfully joined to an aircraft-approved Ti-6Al-4V STD sheet without welding defects using a Nd:YAG laser. The microstructural and mechanical properties of dissimilar laser beam welded Ti-6Al-4V FG-STD butt joints were investigated to (1) describe the effect of alloy compatible filler wire on seam geometry, (2) examine local microtexture and its effect on microhardness, (3) discuss the mechanical behaviour of dissimilar butt joints under static and cyclic tensile load and (4) investigate the fatigue crack propagation (FCP) behaviour.

The condition of the heat affected zones, the laser beam weld and the Ti-6Al-4V FG base material (BM) did not affect the mechanical behaviour of the Ti-6Al-4V FG-STD butt joint under a static tensile load because their strengths (1060 MPa) were higher than that of the Ti-6Al-4V STD BM (1040 MPa). The effect of the strength mismatch was that the plastic deformation of

the laser beam welded Ti-6Al-4V FG-STD butt joint was determined by the lower strength of the Ti-6Al-4V STD BM. The fracture failure of the butt joint under a static tensile load always occurred in the BM. Figure 3-9(a) illustrates local differences in the response of the Ti-6Al-4V FG side, the welding seam and the Ti-6Al-4V STD side to the tensile load of the butt joint. These local differences were measured by applying four measurement marks on the specimen to divide it into three zones and the complete specimen. The FCP behaviour of the laser beam welded FG-STD butt joint was at least comparable to that of the BM sheets (Figure 3-9(b)). The L-T direction of both sheets exhibited slightly lower FCP rates than the T-L direction.

The effect of microstructure and mechanical properties of the dissimilar laser beam welded Ti-6Al-4V FG-STD butt joint on the superplastic formability was assessed in a cone-cup test. The cone-cup test allows the investigation of the SPF-properties of the joint under very similar conditions to those during the real SPF process [4]. The conducted cone-cup test proved the feasibility of SPF of a welded blank with a dissimilar joint. The achieved degree of deformation can be considered to be sufficient for aerospace applications and was not limited by the mechanical properties of the weld or the HAZ. The use of tailored blanks with dissimilar joints can improve the spectrum of applications for SPF of titanium alloy sheets.

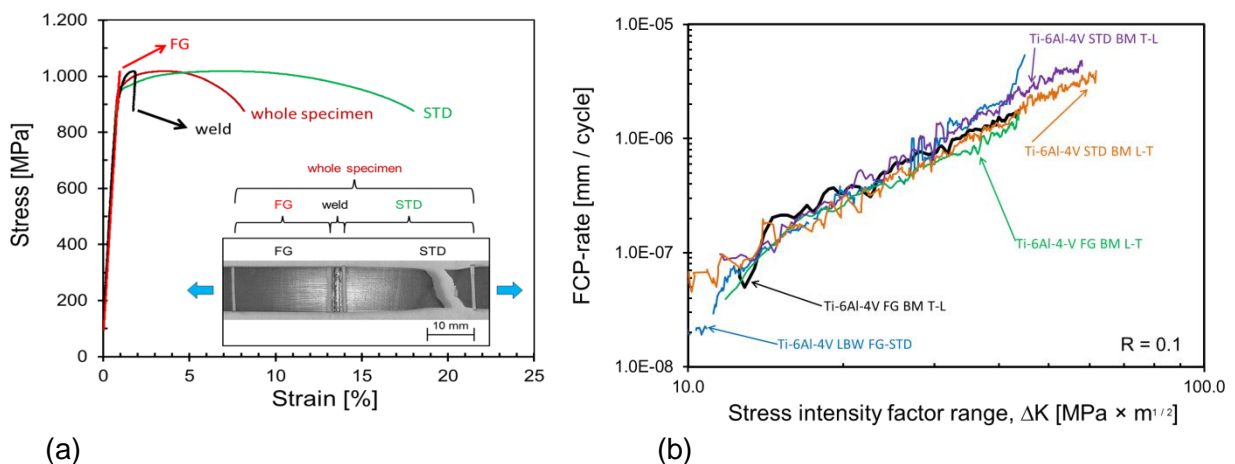


**Figure 3-9: (a) Stress-strain curves of tested Ti-6Al-4V FG and STD BMs and dissimilar laser beam welded FG-STD butt joint; (b) FCP test results.**

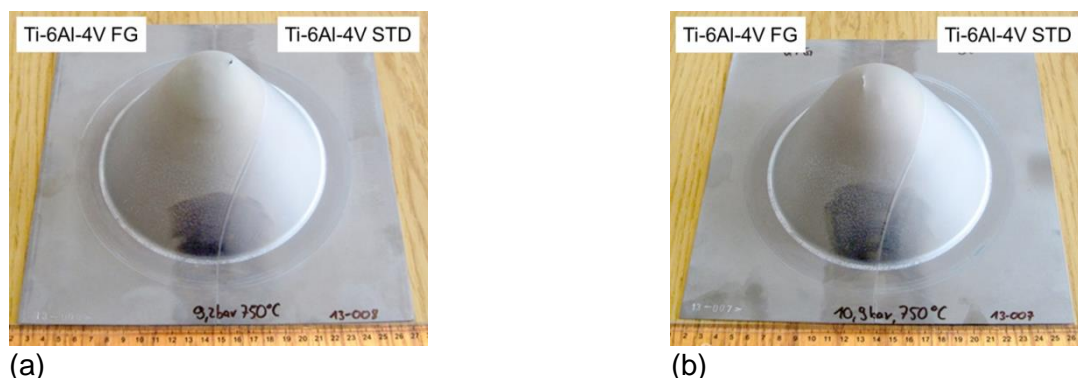


**Figure 3-10: Deformed specimens from the cone-cup test (a) at 0.92 MPa and (b) 1.09 MPa.**

- [1] Salishchev, G.A., Valiakhmetov, O. R., Galeyev, R. M., Froes, F.H. (2004), Materials Science Forum, vols. 447-448, pp. 441-446.
- [2] Final Report to the project “Super-plastic Forming of Titanium Materials at Low Temperatures / CoolTiTech”, funded by the German BMWi under the LuFo IV-3 program, contract no. 20W0905A (2014), FormTech GmbH, Weyhe, Germany.
- [3] Kashaev, N., Ventzke, V., Horstmann, M., Riekehr, S., Yashin, G., Stutz, L., Beck, W. (2015), accepted for publication in Advanced Engineering Materials.
- [4] Beck, W. (2004), Materials Science Forum, vols. 447-448, pp. 145-152.

### **3.6 Biaxial fatigue testing of crenellated fuselage panels**

*J. Lu, N. Huber, N. Kashaev (HZG)*

The efforts to improve the fatigue performance of the airframe structure mainly fall into two categories: enhancing the inherent fatigue resistance of the material itself and optimizing the structural design, such as minimizing the regions of stress concentration and introducing strengthening features like crack retarders and deviators. Unlike conventional crack retarders, which bring additional weight to the structure, the concept of crenellation (Figure 3-11 (a)) [1][2] heightens the fatigue resistance by a systematic thickness variation of the airframe panels while retaining the initial structural weight. In the previous work of Uz et al. [1] crenellations improved the fatigue life of stringer-stiffened panels by over 60% under uniaxial loading conditions. However, for the future applications in industry, this concept still needs further verification in service-related biaxial loading conditions. The influence of materials on the effectiveness of crenellations when applied to different systems of alloy should also be well understood for an accurate assessment of the fatigue performance.

In present work, the fatigue performance of square-shaped flat and crenellated panels (560 mm x 560 mm) both with and without laser-beam-welded stringers is being tested under biaxial loads. Two possible candidate alloys for future aircraft skin – the aluminum–copper alloy AA2139 and the aluminum-lithium alloy AA2198 are used. The specimens are tested using the four horizontal hydraulic actuators of a triaxial testing machine (Figure 3-11 (b) and (c)). The actuators that align in the same axis work in pairs under combined mode of load control. The movement of actuators in one axis is coupled with the other axis to imitate the simultaneous biaxial loading and unloading in the fuselage skin, which is resulted by the cyclic cabin pressurization and depressurization during taking off and landing of the aircraft. The fatigue crack development between prescribed initial and final lengths is monitored by a traveling camera under the specimen. The number of cycles spent during the period is used to estimate the inspection interval that should be implemented in such airframe substructures. The fatigue test results show that the presence of fuselage load parallel to the crack surface can significantly reduce the crack propagation rate (Figure 3-12 (a)). Thus predictions based on uniaxial fatigue tests can lead to over-conservative estimations of the fatigue life of the structure. It was also found crenellations provided much larger percentage of fatigue life improvement under biaxial loading condition compared to the uniaxial loading case (Figure 3-12 (b)).

In conjunction with experimental work, FEM simulations that model the present fatigue tests (Figure 3-11 (d)) are carried out to understand the observed crack propagation behavior and to predict the fatigue life of panels with different crenellation geometry. The stress intensity factors along the crack path are calculated using the FEM models validated by 14 strain gauges attached on the specimen surfaces. In order to improve the prediction accuracy, the possible modification of crack closure behavior by the geometrical change in crenellations and by the application of different materials is considered. The crack opening load is continuously meas-

ured during the experiments by a removable  $\delta_5$  clip gauge at the crack tip, and the data is used in the fatigue life prediction based on the stress intensity factor calculation. The observations from both experiments and simulations provide informative support for further optimization of crenellation patterns and the local material modifications, which can maximize the fatigue resistance of the metallic airframe structure.

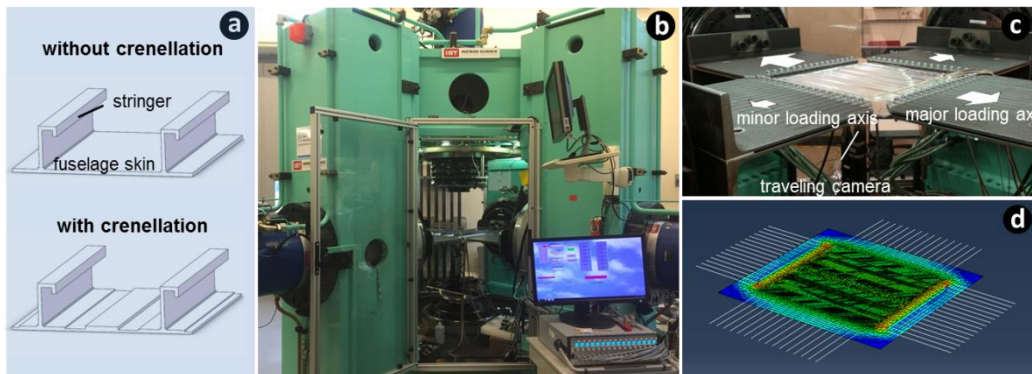


**Figure 3-11: (a) the triaxial testing facility, (b) a detailed view of the experimental set-up and (c) the corresponding FEM model.**

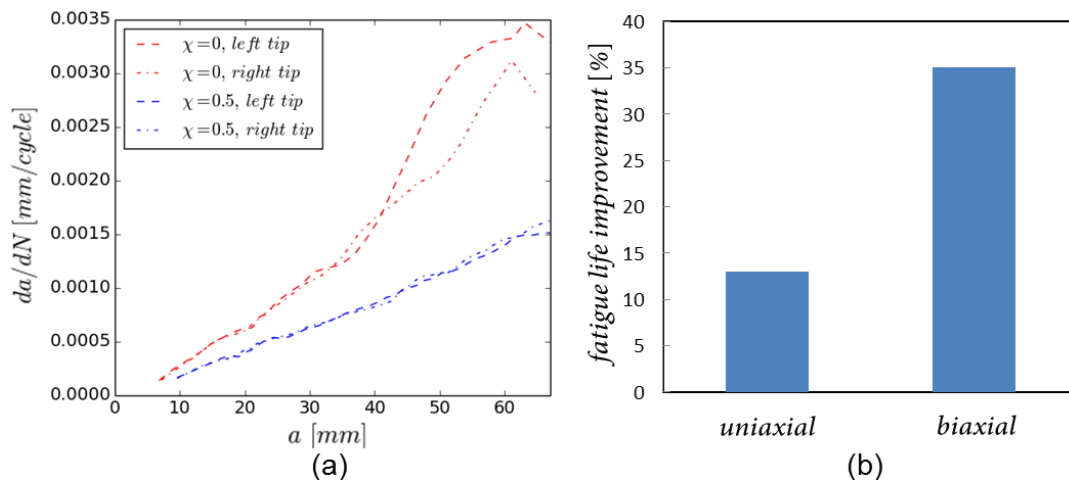


**Figure 3-12: (a) comparison of fatigue crack propagation rate under uniaxial (biaxial load ratio:  $\chi=0$ ) and biaxial ( $\chi=0.5$ ) loading conditions, (b) fatigue life improvement of crenellated panels compare to flat panels under uniaxial and biaxial loading conditions**

- [1] Uz, M.V., Koçak, M., Lemaitre, F., Ehrström, J.C., Kempa, S., Bron, F. (2009), International Journal of Fatigue, vol. 31, pp. 916-926.
- [2] Uz, M.V., Chen, Y.J., Huber, N., (2011), vol. 31, 26th ICAF Symposium - Montreal.

## 4 Fatigue Life Assessment and Prediction

### 4.1 Fracture mechanical investigations of defects and surface roughness on the fatigue performance of additive manufactured Ti-6Al-4V

*D. Greitemeier, C. Dalle Donne (AGI)*

Additive Manufacturing is increasingly considered for manufacturing high quality aerospace parts. Therefore it is essential to cover the full range of material characterization and understand the effects of defects on damage tolerance capabilities. Today this characterisation is at an early stage especially regarding fatigue loads. Only few data are available.

Therefore a test program was set up at Airbus Group to investigate the fatigue performance on titanium grade 5 samples produced by direct metal laser sintering (DMLS) and electron beam melting (EBM) in two surface conditions and two heat treatment conditions. The fatigue life of specimens tested with surfaces in the 'as-built' condition was compared with those tested in the machined condition, highlighting the importance of surface quality with respect to fatigue behavior. In the absence of inherent surface roughness (machined specimens), internal defects such as porosities dominate the fatigue performance. Therefore hot isostatic pressing (HIP) considerably improves fatigue properties.

If typical surface roughness for as shown Figure 4-1 is not removed from the surface, HIP will not improve fatigue properties, since the notch factor of the rough surface nucleates the cracks and is the dominant defect.

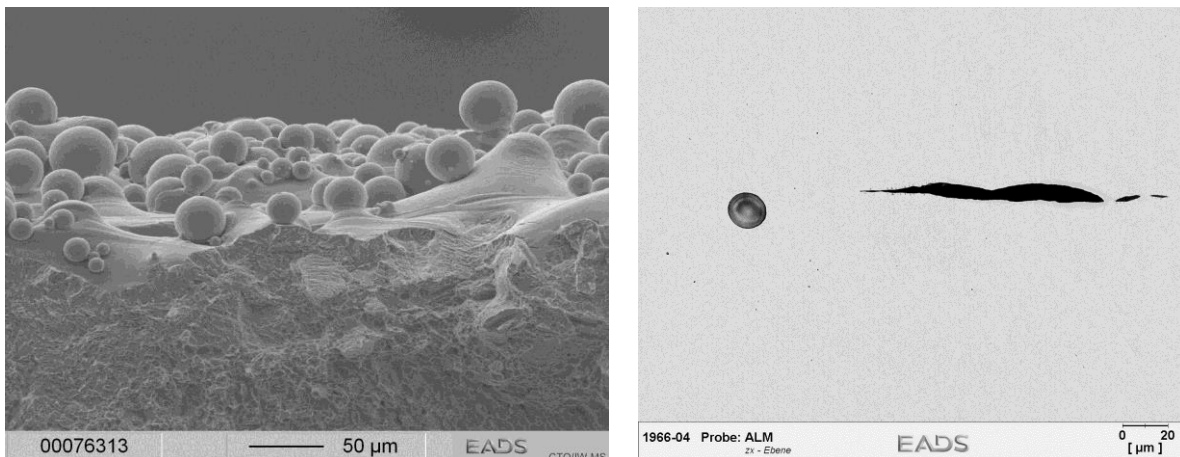


**Figure 4-1: left: typical surface roughness for DMLS, right: typical defects for EBM**

To understand the influence of surface roughness and defects, two models were set up:

1. Influence of defects: A prediction of the effect of defects (e.g. porosity, un-melted spots, lack of fusion or surface roughness) on the fatigue behavior based on a fracture mechanical approach using the  $da/dN - \Delta K$  curve was used. The prediction is therefore based on CT-scans in combination with a Monte-Carlo-Simulation, to predict the SN-curve, including the scatter. The results showed conservative predictions and a distribution which is in good agreement with the experimental results.
2. Influence of surface roughness: a Model was set up to estimate the influence of surface roughness on fatigue, based on an equivalent initial flaw size (EIFS). This EIFS was then used to estimate SN-curves with different surface roughness's. The results are in good agreement with the experimental data.

Furthermore, different surface finishing methods are assessed as an alternative to milling, including vibratory grinding, electro-polishing and plasma polishing. The effectiveness of these methods in terms of fatigue performance will be evaluated within the Airbus Group in future projects.

## 5 Fatigue and Fracture of Metallic Fuselage Materials

### 5.1 Enhancement of the fatigue properties of the metastable $\beta$ titanium alloy Ti 38-644 by obtaining a superior microstructure via Thermohydrogen Treatment (THT)

*V. Macin, H.-J. Christ (LMW)*

Excellent corrosion resistance, reasonable room temperature formability and very good fatigue endurance make the highly stabilized (solute-rich)  $\beta$  titanium alloys attractive materials for fatigue critical components in structural aerospace applications requiring high strength as well as low weight at the same time. In this context, the applicability range of  $\beta$  titanium alloys might be restricted due to their proneness to an inhomogeneous precipitation of the strengthening  $\alpha$  phase within the  $\beta$  microstructure and the formation of soft  $\alpha$  phase layers along the  $\beta$  grain boundaries ( $\alpha_{GB}$  phase). The formation of precipitate-free zones (PFZ) and the  $\alpha_{GB}$  phase are known to be microstructural key features determining the life of highly stabilized  $\beta$  titanium alloys since monotonic and cyclic plastic deformation are concentrated in these weak regions. With increasing yield strength of the material, such microstructure phenomena control fatigue crack initiation as well as fatigue crack propagation [1,2]. This alloy class can be heat-treated to a broad range of strength to ductility ratios, whereby duplex aging consisting of the low and high temperature aging is despite the complexity the best conventional heat treatment to establish a more homogeneous distribution of strengthening  $\alpha$  precipitates [3].

Increasing demands for better performance of components and structures necessitate innovative routes of thermomechanical processing. In the present, study using hydrogen as a temporary alloying element within the heat treatment, referred to as Thermohydrogen Treatment (THT), facilitates the improvement of mechanical properties of the highly stabilized  $\beta$  titanium alloy Ti 38-644 ( $\beta$ -C) by means of microstructure modification, because  $\beta$  titanium alloys feature excellent characteristics concerning kinetics and thermo-dynamics of hydrogen sorption. According to Figure 5-1a, the THT strategy *hydride-induced alteration of dislocation arrangement* (HADA) contains five treatment steps: recrystallization, diffusion controlled hydrogenation, hydride formation based on the hydrogen-induced redistribution of alloying elements, dehydrogenation and aging [4]. The volume effects associated with hydride formation lead to local matrix deformation accompanied by accumulation and pile-up of dislocations. The hydride-induced change of the dislocation arrangement is still present after hydride dissolution and complete hydrogen release during dehydrogenation. Hydride-induced  $\beta$  crystal lattice distortion intensifies the precipitation of refined homogeneously distributed  $\alpha$  particles without any formation of  $\alpha_{GB}$  phase (see Figure 5-1b). In contrast, the optimized time-consuming duplex aging leads to the formation of micro-PFZ accompanied by a nucleation and a growth process of the acicular  $\alpha$  phase (see Figure 5-1c).

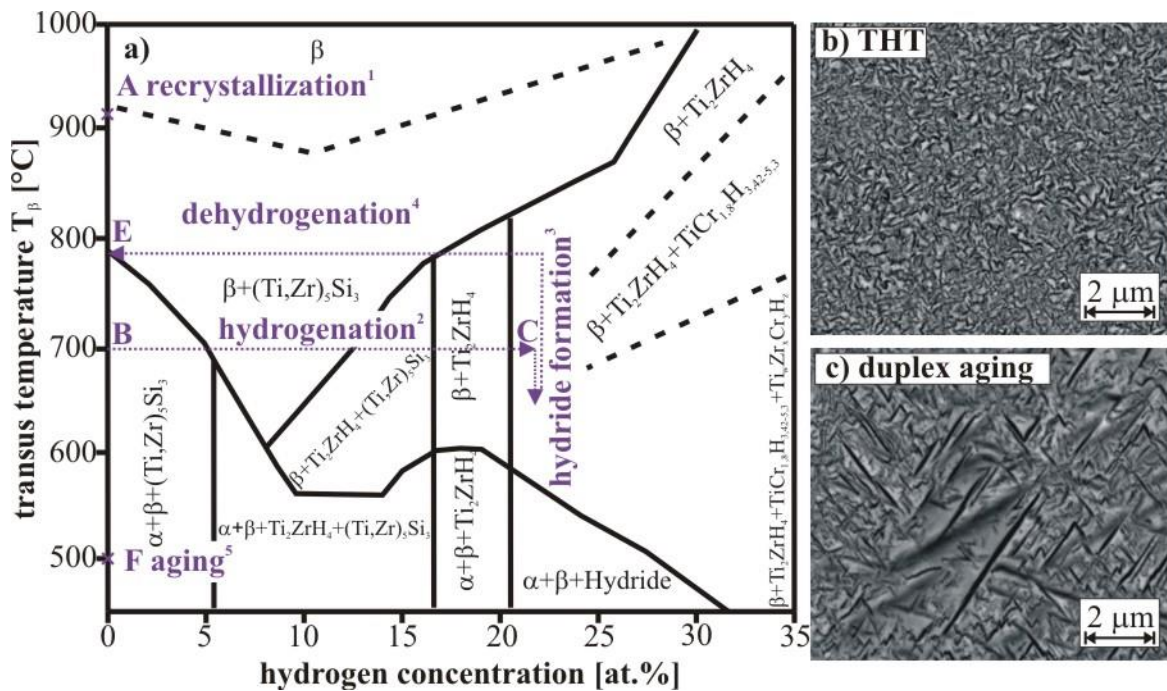


Figure 5-1: )  $T_{\beta}$  as function of the hydrogen content; HADA-THT strategy of  $\beta$ -C is marked schematically by ABCDEF; b) microstructure finally obtained after 5-step HADA-THT; c) reference microstructure after duplex-aging cycle

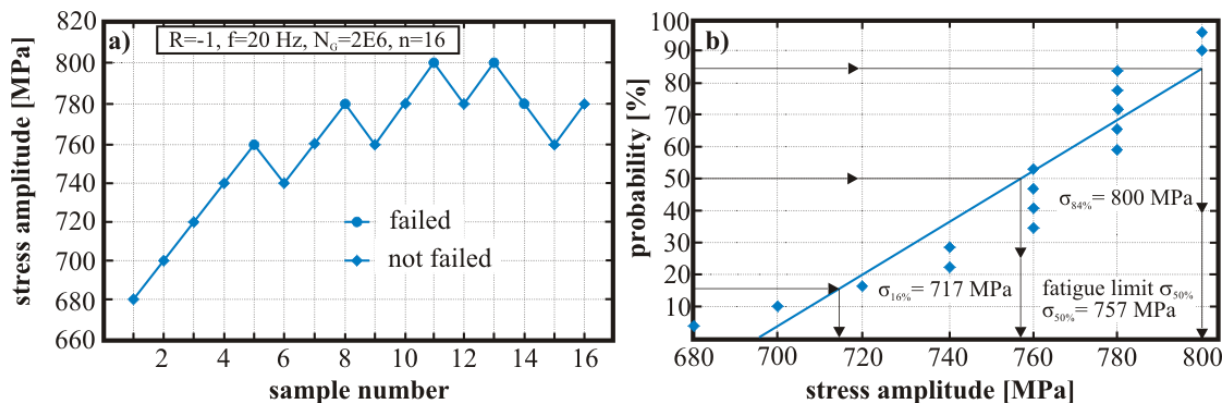


Figure 5-2: Results of the staircase test applied to the 5-step HADA-THT treated  $\beta$ -C a) sequence of tests, b) statistical evaluation

Fatigue tests were performed under symmetrical tension-compression conditions. The fatigue limit of 757 MPa and the standard deviation of 41.5 MPa for an ultimate number of load cycles  $N_G = 2 \times 10^6$  were determined statistically according to the modified staircase method (see Figure 5-2). The enhancement of the fatigue limit of about 11% compared to the duplex-aging cycle ( $\sigma_{50\%} = 700$  MPa) is based on the suppression of the  $\alpha_{GB}$  formation as well as the refinement of the acicular  $\alpha$  phase, meaning significantly reduced intermediate spacing between the platelets, and the associated prevention of micro-PFZ. Long crack propagation of single edge notch bend (SENB) samples was studied under 4-point bending loading according to ASTM E-647. A fatigue crack growth threshold of about  $2.7 \text{ MPa m}^{0.5}$  was determined at a stress ratio of  $R = 0.1$

according to the load shedding method. In comparison to duplex aging, the  $\Delta K_{th}$ -value decreased marginally by about  $0.2 \text{ MPam}^{0.5}$ .

- [1] Peters M, Leyens C. Titan und Titanlegierungen. 3th ed. Weinheim: WILEY-VCH Verlag; 2002.
- [2] Lütjering G, Williams JC. Titanium. 2th ed. Berlin: Springer-Verlag; 2007
- [3] Schmidt P, El-Chaikh A, Christ H-J. Effect of duplex aging on the Initiation and propagation of fatigue cracks in the solute-rich metastable  $\beta$  titanium alloy Ti 38-644. Metall Mater Trans A 2011;42(9):2652-67.
- [4] Schmidt P, Macin V, Christ H-J. Thermohydrogen treatment of highly beta-stabilized titanium alloy Ti 38-644 (Beta-CTM). In: Somerday BP, Sofronis P, editors. Hydrogen-materials interactions. New York: ASME; 2014, 661-8.

## 5.2 Hydride-induced improvement of fatigue properties of the high-strength $\beta$ titanium alloy Ti 10-2-3 by Thermohydrogen Treatment (THT)

V. Macin, H.-J. Christ (LMW)

The high-strength near- $\beta$  titanium alloy Ti 10V-2Fe-3Al (Ti 10-2-3) exhibits excellent hot forgeability and hardenability up to 125mm thickness, high toughness in air and salt water environments at temperatures up to 315°C as well as creep-stability characteristics close to the  $\alpha+\beta$  alloys. With regard to the application requirements, this alloy can be heat-treated to a wide strength-toughness range correlated with its bimodal microstructural characteristics [1]. Ti 10-2-3 developed for the use in the aerospace industry, where the near-net shape forging process is applied in the landing gear structure of the Boeing 777, cargo handling fittings, and Super Lynx helicopter rotor head [2].

In order to broaden the applicability range of Ti 10-2-3, innovative routes of thermomechanical processing are necessary. The object of the present study is the hydrogen-induced microstructure modification by means of Thermohydrogen Treatment (THT) in order to improve the mechanical properties under monotonic and cyclic loading conditions. The formation of hydrogen-induced phases precipitating preferentially at grain and phase boundaries as a consequence of hydrogen supersaturation and eutectoid decomposition play an essential role in the successful implementation of THT. The THT process *hydrogen-induced recrystallization of  $\beta$  phase* (HIRB) shown schematically in Figure 5-3a comprises five treatment steps: solution treatment, hydrogenation accompanied by the precipitation of the hydrogen-induced phase (Fig. 1b), recrystallization (Fig. 1c), dehydrogenation and aging [3]-[4]. The diffusion-controlled hydride formation ( $\text{TiFeH}$  and  $\text{TiFeH}_2$ ) accompanied by a volume expansion up to 25% [5] causes crystal lattice distortion around hydrides associated with an increased dislocation density. The recrystallization of the  $\beta$  phase accompanied by the complete hydride decomposition can be related to the high dislocation density comparable to the condition after cold working. In comparison to the technical heat treatment, the HIRB-THT process results in the minimized volume fraction of  $\alpha_{GB}$  phase and completely dissolved globular  $\alpha_P$  phase accompanied by a suppression of the  $\beta$  grain coarsening. The increased age hardening of the fine-grained  $\beta$  matrix and the reduced volume fraction of  $\alpha_{GB}$  phase may improve the fatigue strength in the HIRB-THT condition.

Figure 5-4 shows the results of fatigue tests performed under symmetrical tension-compression conditions according to the modified staircase method. Fatigue testing of THT-treated samples

is in progress. In contrast to our expectations, the improvement of fatigue life is not strongly pronounced by the hydride-induced microstructure modification that can be related to the observed preferred  $\beta$  crystal orientation after hydrogen-induced recrystallization.

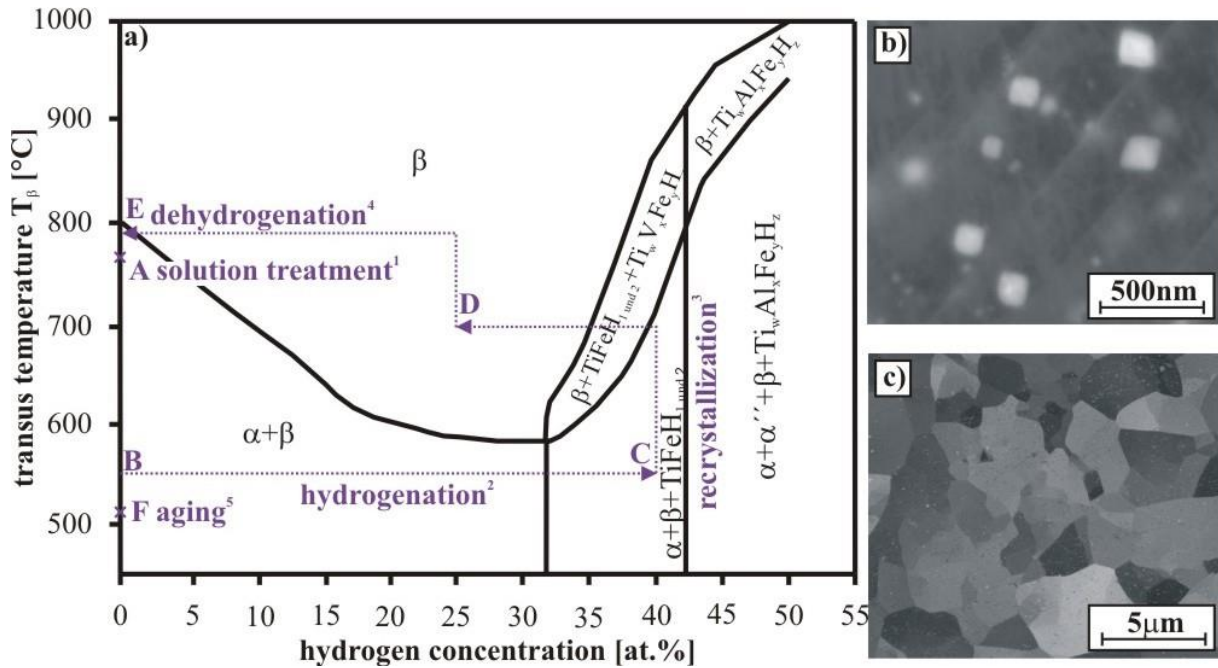


Figure 5-3: a) HIRB-THT strategy inscribed schematically by ABCDEF in the  $T_{\beta}$  diagram; FE-SEM micrographs after THT-steps b) hydrogenation (BC) and c) recrystallization (CD)

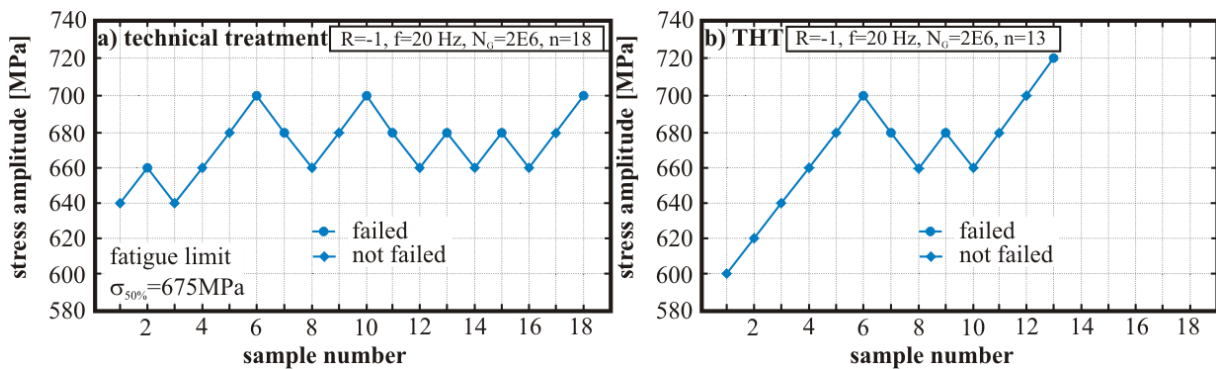


Figure 5-4: Results of the staircase test applied to a) conventional technical heat treatment as reference condition and b) 5-step HIRB-THT treated material (sequence of tests)

Fatigue crack initiation at the sample surface indicated a microstructural homogeneity after the HIRB-THT process. The fatigue crack propagation measurements of single edge notch bend (SENB) samples are taken according to ASTM-E647 under cyclic 4-point bending loading. The determination of long crack growth behavior at a stress ratio of  $R = 0.1$  according to the load shedding method indicated that the fatigue crack growth threshold  $\Delta K_{th}$  in the peak-aged HIRB-THT condition is below  $2.0 \text{ MPam}^{0.5}$ . The crack propagation resistance of the technical heat treated condition is  $2.3\text{-}3.5 \text{ MPam}^{0.5}$ . As expected, the hydride-induced precipitation hardening of the  $\beta$  matrix of the HIRB-THT condition causes no improvement of the long crack growth be-

havior, which is generally deteriorated by the precipitation hardening of the  $\beta$  matrix. This is characteristic of precipitation-hardenable  $\beta$  titanium alloys.

- [1] Boyer R, Welsch G, Coolings EW. Material properties handbook: titanium alloys. 4th ed. Materials Park: ASM International; 1994.
- [2] Lütjering G, Williams JC. Titanium. 2th ed. Berlin: Springer-Verlag; 2007
- [3] Macin V, Christ H-J. Hydride-induced microstructure optimization of high-strength beta titanium alloy Ti 10-2-3 by thermohydrogen treatment. In: Proceedings of the LightMat 2013, <http://www.dgm.de/dgm/lightmat/>: DGM; 2014, 1-6.
- [4] Macin V, Schmidt P, Christ H-J. Thermohydrogen treatment of high strength beta titanium alloy Ti 10V-2Fe-3Al. In: Somerday BP, Sofronis P, editors. Hydrogen-materials interactions. New York: ASME; 2014, 669-76.
- [5] Lewkowicz I. Titanium-Hydrogen. Solid State Phenom 1996;49-50:239-80.

### **5.3 Laser Shock Peening as Surface Technology to extend Fatigue Life in Metallic Airframe Structures**

*D. Furfari, N. Ohrloff (Airbus) and E. Hombergmeier, U. C. Heckenberger, V. Holzinger (AGI)*

The use of surface technologies inducing residual stresses can be employed in aeronautical industry as technologies to ensure salvage for identified hot spots in terms of fatigue and crack growth performance. Degradation processes, such as fatigue, limit service lives of aircraft structures. Technologies and methodologies that improve the resistance of structures to these degradation processes are of benefit to the aircraft industry in terms of extending the service life of the structure and thus reducing maintenance costs. An emerging technology is Laser Shock Peening, which can be used in lieu of conventional Shot Peening to introduce residual compressive stresses to a metallic structure. This engineering field can be identified as Residual Stresses Engineering aiming at improving the economic and ecological impact of an aging fleet as well as of future aircraft structures by controlling the residual stresses.

This chapter provides an overview how this technology can enhance fatigue and crack growth for different metallic materials commonly used in aircraft structures: ranging from Al alloys (2024-T351, 7010-T7451, 7050-T7451) to Precipitation Hardened Stainless Steel X3CrNiMoAl13-8-2. The depth of the compressive residual stresses is controlled by the laser peening parameters to obtain the “desirable” residual stress profile with the aim to inhibit fatigue crack initiation and crack propagation as function of the thickness. Through thickness compressive residual stresses can be obtained treating the two opposite surfaces of Al sheets (i.e. Al2024 and Al7050) up to a thickness of 6 mm, controlling the extension of the tensile residual stresses (auto balanced stresses) outside the processes areas to avoid undesirable increase of stresses at other critical locations. Both Al2024-T351 clad and unclad material (2 mm thick) where laser peened and fatigue tested under constant amplitude loading showing the capability to slow down through thickness crack growth when the crack front crossed the compressive residual stress field. It was possible to obtain through thickness compressive stresses firing the laser directly onto the Al clad layer at the surface of the specimens without prior clad layer removal. The residual stress field induced by the laser shock peening process was characterized with hole drilling technique as well as non-destructive testing such as X-Ray Diffraction and Synchrotron diffraction. Tests on CCT (Centre Crack Tension) specimens made of Al2024-T351

have shown a dramatic reduction of the crack propagation rates (an order of magnitude compared with reference material) at a stress intensity factor ranging from  $30 \text{ MPam}^{1/2}$  to  $50 \text{ MPam}^{1/2}$  (see Figure 5-5).

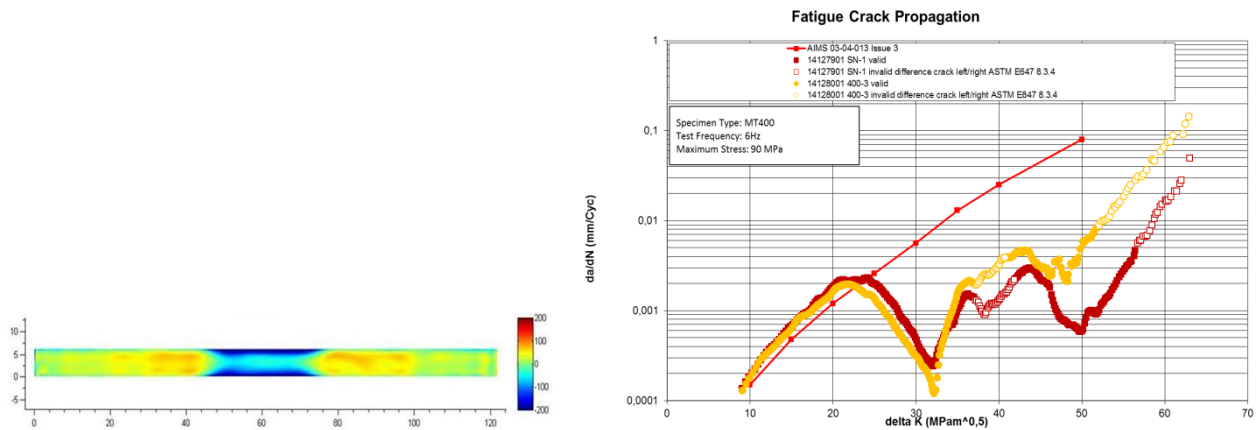


**Figure 5-5: Example of through thickness compressive residual stress in Al alloys up to 6mm thickness laser shock peened, from both sides (left) and crack growth behavior ( $da/dN$  vs.  $DK$  curve) in Al2024-T351 after LSP treatment (right).**

Most works on LSP have utilized a Neodym-YAG laser with its fundamental wavelength of 1064 nanometers in the near infrared or Neodym glass lasers (fundamental wavelength at 1054 nanometers) in combination with an applied absorption/insulation layer (usually a thin aluminum foil). This additional Al layer, which vaporizes during the laser pulse forming the plasma pressure and the consequent pressure shock wave travelling into the material, is also used to prevent the surface from melting or being damaged during peening (as a sort of sacrificing layer). When the laser process was used without the prior application of the Al ablative layer (i.e. laser peening onto bare material) the status of the surface was studied and it was found that the thermally affected layer caused by the high temperature during the peening (although only for a duration of 20 nanoseconds) left the first 5-10  $\mu\text{m}$  of material without compressive residual stress or slightly in tension. A laser peening coverage above 300 % brought back the compressive residual stresses at the near surface of the treated material. For high production rates or to make the application of laser shock peening in some specific aircraft components economical more attractive it could be a valid solution to carry out the treatment without ablative coating which is normally a manual operation slowing down the manufacturing rate significantly.

Surface treatments such as Chromic Acid Anodizing (CAA) and Tartaric Sulfuric Anodizing (TSA) are typical surface protections applied in Al structures to prevent from corrosion damages. Structural coupons made of Al7050-T7451 and Al7010-T7451 of 30 mm thickness containing a stress concentration factor of 2 and the surface treatments above described were fatigue tested under constant amplitude loading with stress ratios of:  $R=-3$ ,  $R=-1.75$ ,  $R=-1$ ,  $R=-0.3$  and  $R=0.1$ . Deep compressive residual stress induced on the surface by laser shock peening (minimum 3 mm depth) demonstrated to be able to delay the fatigue crack initiation and the crack propagation in all ranges of R ratios tested providing for all conditions a significant fatigue life extension compared to conventional shot peening and ultra-sonic peening. The fatigue behavior was also studied in presence of the anodizing layer. The capability of inducing deep residual stresses, firing laser shock peening directly onto the surface coating without prior removal, is an attractive alternative to the standard operation. The test campaign was completed with Constant Amplitude fatigue tests demonstrating the capability of laser shock peening to delay the crack initiation and propagation compared to non-treated structural coupons. The fatigue life of the

laser shock peened condition could be increased by a factor of more than 10, even compared to the shot peened condition (Figure 5-6).

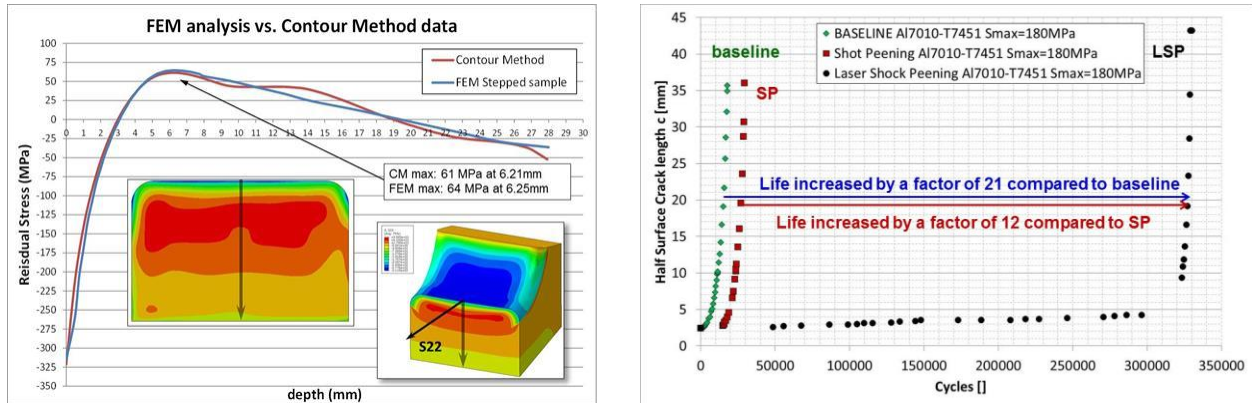


Figure 5-6: Through the thickness residual stress profile (left) and crack growth curve under constant amplitude loading (R=0.1) in Al7010-T7451 30mm thick plate.

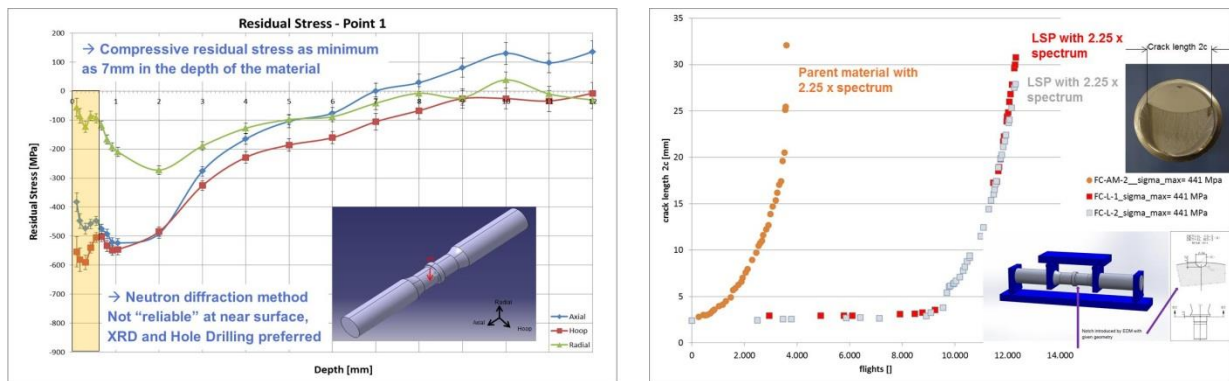


Figure 5-7: Crack propagation curves determined under spectrum loading in as machined and laser shock peened condition.

Precipitation Hardened Stainless Steel X3CrNiMoAl13-8-2 has been selected, as typical high strength material commonly used in aeronautic structures, to investigate the fatigue and crack growth behavior after inducing compressive residual stress at the near surface by means of laser shock peening. Residual stress measurements on round bar coupon of 35 mm diameter using hole drilling and neutron diffraction techniques demonstrated the capability to introduce high compressive residual stresses at the near surface (-0.8 YST of the material) with depth into the material of minimum 2 mm. The effect of surface layer removal by fine machining (i.e. roughness of 0.8  $\mu$ m) after laser peening without ablative layer has been investigated. The effect on fatigue of laser peening without ablative coating and fine surface machining as well as with ablative layer without surface machining has been investigated to assess the fatigue behavior in unnotched flat coupons as well as round bar coupons having a stress concentration factor of 2 subjected to four point bending loading. The surface condition after laser peening with surface protection (ablative layer) in terms of roughness profile has been studied. The crack growth behavior in deep residual stress field was part of the investigation and the experimental results are shown in Figure 5-7. The specimens used for this type of test were round bar coupons with a stress concentration factor of 2 subjected to four point bending fatigue loading at variable amplitude loading condition. The initiation site at the stress concentration area was ad-

dressed by an EDM notch of 2.54 mm x 1.27 mm prior to fatigue pre-cracking. Potential drop and optical techniques were used to monitor the crack growth as well as fracture surface investigations by SEM after the fatigue crack propagation test.

## 6 Fatigue and Fracture of Engine Materials

### 6.1 High-temperature low cycle and thermomechanical fatigue behaviour of titanium aluminides

*A. El-Chaikh, H.-J. Christ (LMW)*

In recent times,  $\gamma$ -TiAl-based alloys have found large-scale implementation as blade material into advanced aero engines, substituting heavy-weight nickel-based alloys. A remaining crucial issue is however to assess the material's maximum reliable fatigue and to develop a suitable fatigue life prediction model for both low cycle fatigue (LCF) and thermomechanical fatigue (TMF) conditions.

Investigations conducted at the authors' institution have revealed that the high-temperature low cycle fatigue behaviour of the advanced  $\gamma$ -TiAl-based alloy TNB-V2, containing 8 at.-% niobium, is rather modest at an applied total strain amplitude of  $\Delta\epsilon/2 = 0.7\%$  under fully-reversed testing conditions. In the temperature field between room temperature and 850°C, fatigue life never exceeded 600 cycles.

Recent results on the LCF and TMF behaviour of TNB-V2 at lower strain amplitudes show a significant increase in the fatigue life. The different fatigue performance can be correlated with the amount of plastic strain amplitude. The amount of plastic strain amplitude almost doubles between total strain amplitudes from 0.6 to 0.7%. In this study a model was developed to predict the fatigue life of  $\gamma$ -TiAl-based alloy TNB-V2 under LCF and TMF conditions. In the first part of this model the TMF hysteresis loop was simulated by means of a multi-component model using only the LCF data. In order to simulate the hysteresis loops for the complete test microstructure changes as well as hardening and softening processes were integrated. Figure 6-1 shows a comparison between a simulated and obtained TMF hysteresis loop at the beginning of the test as well as at the half of the fatigue life ( $N_f/2$ ).

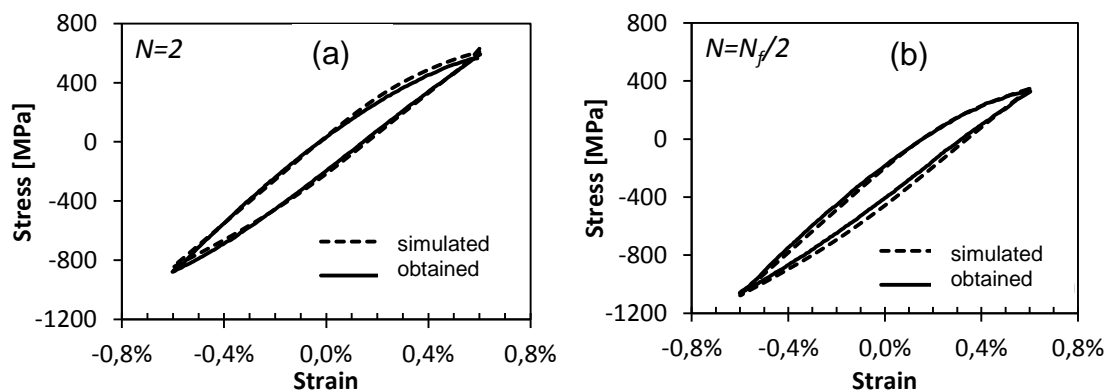


**Figure 6-1: Suitable agreement between simulated and obtained TMF hysteresis loop at the beginning (a) of the test as well as at the half (b) of the fatigue life ( $N_f/2$ ).**

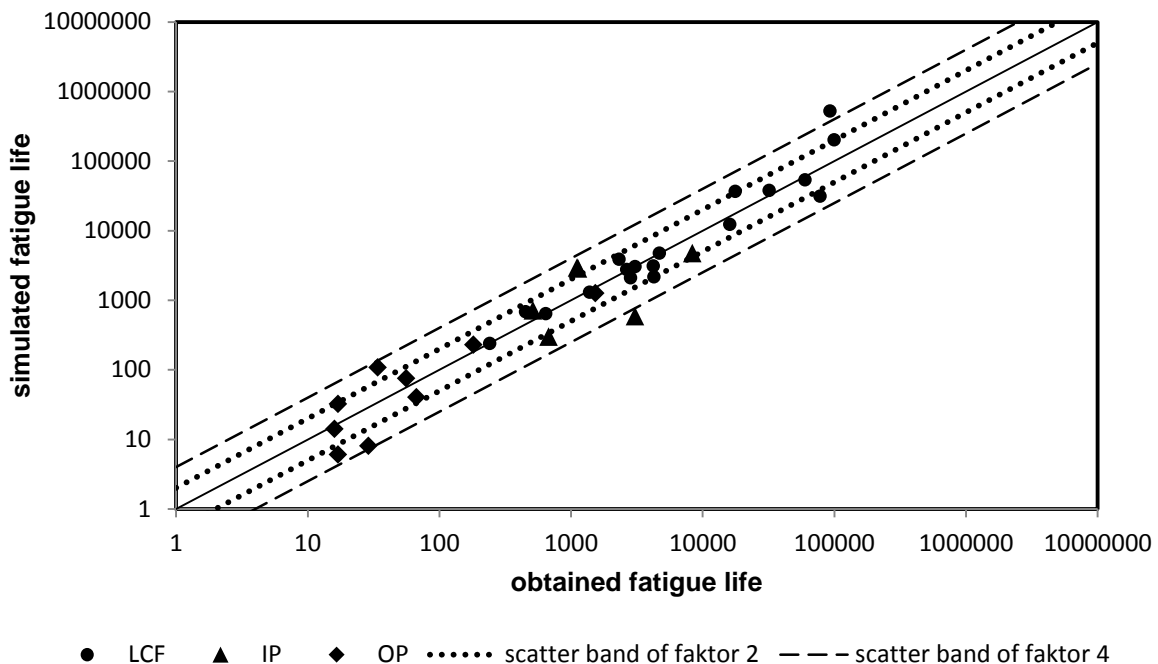


**Figure 6-2: Comparison between the obtained and the calculated fatigue life under TMF and LCF conditions.**

In the second part of the model a damage parameter (equation 1) was defined, which includes the temperature as a physical dimension and takes into account the effect of the mean stresses.

$$P_{Ges} = \frac{p_{max} + p_{min}}{2} + p_m^{\alpha_{Rp}} = \frac{1}{2} \left( \frac{\sigma_{ZUP}}{R_{p0,2}(T_{\sigma_{ZUP}})} + \frac{\sigma_{DUP}}{R_{p0,2}(T_{\sigma_{DUP}})} \right) + p_m^{\alpha_{Rp}} \quad \text{equation (1)}$$

Where  $p_{max}$ ,  $p_{min}$  und  $p_m$  are the damage factors caused by tension stress, compression stress and mean stress, respectively,  $\sigma_{ZUP}$  and  $\sigma_{DUP}$  are the stress at the tensile reversal point and compression reversal point, respectively,  $\alpha_{Rp}$  is a material depending coefficient.

The parameters in terms of upper and lower stresses needed for this model were calculated by means of the multi-component model mentioned above. The results of the fatigue life prediction model under LCF and TMF conditions are shown in Figure 6-2.

## 6.2 Influence of fatigue frequency and hold-time on the crack propagation in IN718 in the temperature range of dynamic embrittlement

*K. Wackermann, U. Krupp, H.-J. Christ (LMW)*

IN718 is a standard nickel-based alloy for high-temperature usage in gas turbines or turbochargers since it combines good mechanical properties with reasonable material cost. At elevated temperature IN718 is prone to cracking by dynamic embrittlement. Dynamic embrittlement is caused by temperature and tensile stress assisted oxygen grain boundary diffusion. This results in fast and intercrystalline crack propagation rate whereas reference tests in vacuum or inert gas show slower transcrystalline crack propagation. Furthermore, the fatigue frequency or

the dwell-time, which is the holding time at maximum load in a fatigue cycle, affect the crack propagation rate and fracture morphology. The longer the dwell-time the faster is the crack propagation rate due to higher oxygen diffusion. Especially the correlation of fracture morphology and crack propagation rate is not fully understood yet and is therefore the objective of this study.

A servohydraulic test rig with induction heating and an alternating current potential drop system (ACPD) to measure the crack propagation rate was used. A vacuum chamber allowed reference tests in vacuum. Isothermal tests were performed on corner crack specimen at 650°C and a load ratio of  $R = 0.1$ .

So far, tests in laboratory with sinusoidal load at 1 Hz and 4 Hz and dwell-time test with cycle times of 7 s, 30 s, 100 s and 300 s were performed. The cycle time in the dwell-time tests is divided into loading, unloading and the dwell-time. For example in the 300 s dwell-time test there are 2 s for loading, 296 s dwell-time and 2 s unloading. The test is named accordingly 2-296-2. As reference a fatigue frequency of 1 Hz was selected for a test in vacuum. As expected the crack propagation rate increases with increasing dwell time or decreasing frequency as there is more time for oxygen diffusion in one loading cycle, see Figure 6-3. For long dwell times an intercrystalline crack propagation is observed. At intermediate cycle times, ranging from 0.25 s (Test: 4 Hz air) to 7 s (dwell-time test: 2-3-2), a continuous change from a transcrystalline fracture morphology at short cycle times to an intercrystalline fracture morphology for long cycle times is observed, see Table 6-1. In the reference test in vacuum a pure transcrystalline fracture is observed.

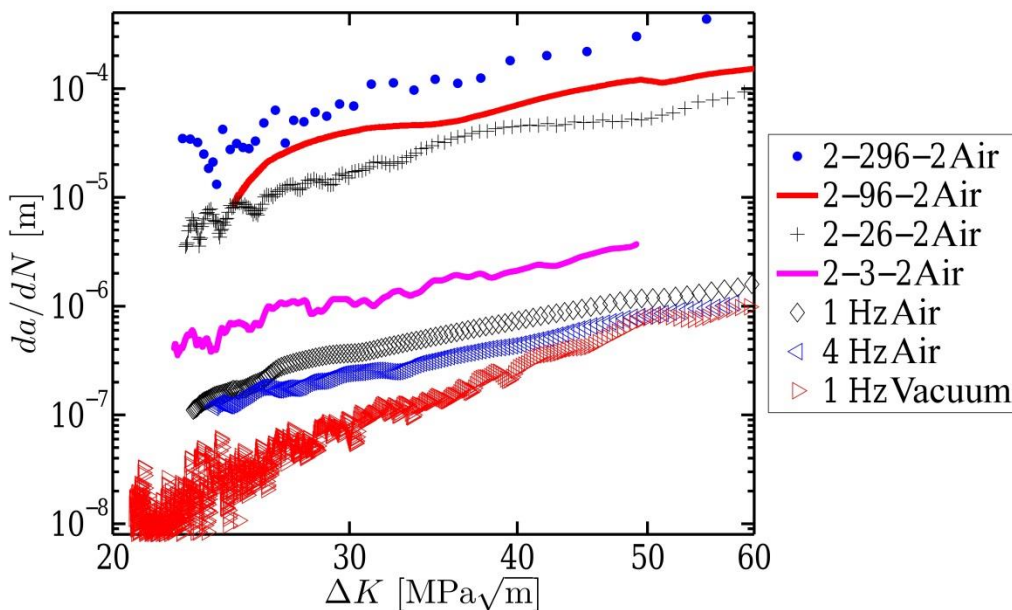


**Figure 6-3: Crack propagation rates at 650°C with a load ratio of  $R = 0.1$  tested in air and vacuum. The load was either applied sinusoidal at 1 Hz and 4 Hz or in a dwell-time test with dwell-times of 3 s, 26 s, 96 s and 296 s and load ramps of 2 s.**

Based on the results of these tests a model mechanism for the crack propagation is proposed. In the regime of transcrystalline fracture at high test frequencies it is assumed that the crack driving force is the fatigue damage. Therefore, the crack propagation is modelled by Paris's Law. For long dwell-times with a pure intercrystalline fracture it is assumed that the crack driving force is the diffusion controlled dynamic embrittlement. The crack propagation in this damage

regime is modelled by simple diffusion mechanisms. In the intermediate regime a mixture of dynamic embrittlement and fatigue damage is the crack driving force. It is assumed that the ratio of the two fracture morphologies - which can be measured on the tested specimen - can be used to weight the two damage mechanism in the intermediate damage regime. The comparison of the measured and the modelled crack propagation rates correlate well. Therefore, there is evidence that the dynamic embrittlement and the fatigue damage are two interacting damage mechanism whose occurrence probabilities depend on the cycle time.

**Acknowledgment**

The financial support by Deutsche Forschungsgemeinschaft (DFG, grant No. KR1999/7) is gratefully acknowledged.

**Table 6-1: Percentage of measured intercrystalline fracture for crack propagation test at 650°C at a stress ratio of R = 0.1 in laboratory air for two sinusoidal load modes at frequencies of 1 Hz and 4 Hz and a dwell times test with a dwell time of 3 s and load ramps of 2 s.**

$\Delta K$ [Mpa $\sqrt{m}$ ]	2-3-2 Air	1 Hz Air	4 Hz Air
28.5	93%	43%	25%
37.3	74%	30%	9%
44.0	75%	24%	5%
51.8	72%	14%	2%

**6.3 High temperature low cycle fatigue testing technique for miniature specimens from single crystal super alloys for gas turbine blades**

*C. Meid, U. Waedt, A. Subramaniam, J. Wischek, M. Bartsch (DLR)*

Gas turbine blades for the high pressure turbine of aeroengines are made of single crystalline Ni-based super alloys. In service they have to sustain complex creep and fatigue loads at high temperatures. For the investigation of crack initiation sites and elementary deformation mechanisms under high temperature fatigue a miniaturized testing technique has been developed, which allows to perform low cycle fatigue tests on specimens with a length of only 20 mm (Figure 1a).

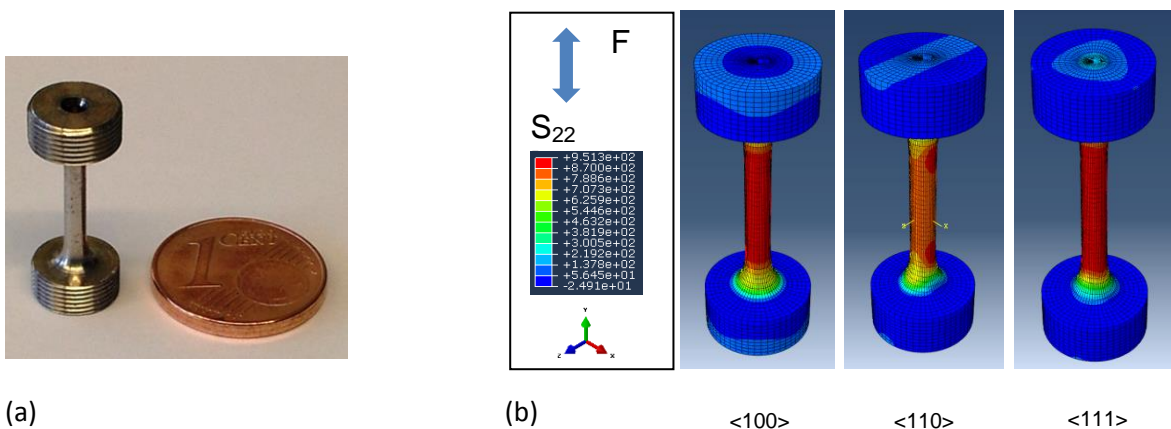


**Figure 6-4: Miniature specimen for high temperature fatigue tests (a) macro photograph and (b) stress distribution for specimens with length axis in different crystallographic orientations under tensile load (stress component  $S_{22}$  in loading direction shown).**

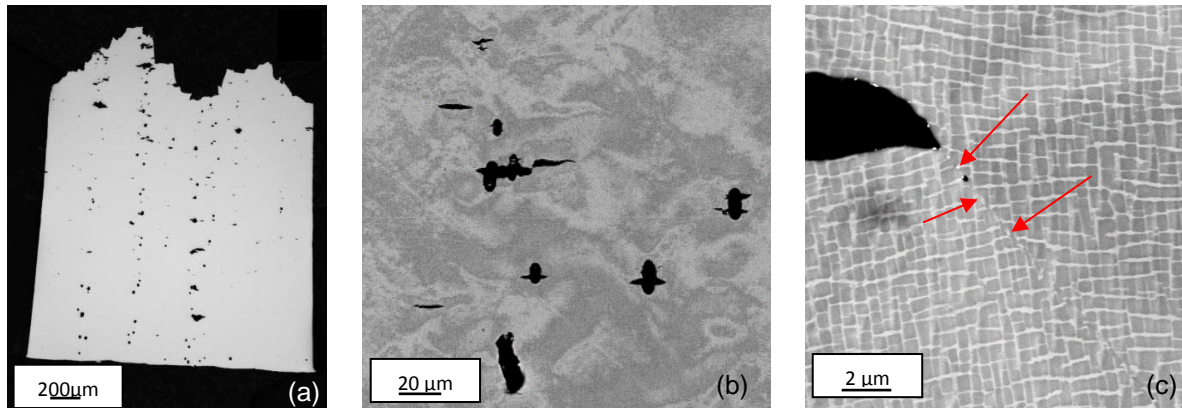


**Figure 6-5: Cross sections of specimen after LCF at 950°C. (a) Overview of pore chains aligned along solidification dendrites. (b) Multiple crack growth at internal pores. (c) Deformation band at crack tip along  $\langle 111 \rangle$  plane of the single crystal,  $\gamma'$ -precipitates were sheared and small intermetallic precipitates (see arrows) occurred..**

The development of miniature specimens was driven by several reasons: (1) More specimens can be prepared from one cast plate, e.g. from one single crystal cast plate with dimensions of (110 x 100 x 20) mm<sup>3</sup> about 6 standard specimens can be manufactured but, depending on the selected crystallographic orientation, 20 to 60 miniature specimens. (2) It is more difficult to avoid defects such as small parasite grains, so called freckles, in standard size than in miniature specimens. Such defects may superpose the effects of microstructural features such as microporosity or  $\gamma/\gamma'$ -microstructure. (3) Depending on the crystallographic orientation of the cast plate it may be not possible to prepare standard size specimens for all crystallographic directions of the cubic (fcc) crystal.

The specimen geometry has been optimized in such a way that for specimens with the length axis parallel to one of the 3 main crystallographic orientations  $\langle 100 \rangle$ ,  $\langle 110 \rangle$ , or  $\langle 111 \rangle$  of the cubic crystal system the maximum stress will occur within the measurement length (Figure 6-4). For the geometry optimization temperature dependent elastic material properties of CMSX-4 after precipitation hardening were used [1, 2]. The safety factor against buckling is 7.6 and thus similar to that of standard size specimens as described e.g. in [3]. For clamping a fixture has been designed, which ensures a change of load sign free from backlash.

First experiments have been performed at 950°C under load control with triangular wave form and a frequency of 0.25 Hz, constant stress amplitude of 160 MPa, positive R-ratio, and maximum tensile stresses from 680 to 740 MPa. The specimen length axis was parallel to the crystallographic  $\langle 100 \rangle$  direction and parallel to solidification direction. The number of cycles to failure was dependent on maximum stress, and all specimens did fracture within the measurement length. Cracks initiated at pores aligned along the solidification dendrites within the interdendritic space (Figure 6-5 a,b). These pores were generated during solidification and further thermal treatment. At crack tips deformation bands along the  $\langle 111 \rangle$  planes of the crystal occurred.

Shearing of  $\gamma'$ -precipitates and precipitation of intermetallic phases on the  $\langle 111 \rangle$  planes were observed (Figure 6-5,c).

The developed miniaturized high temperature LCF testing technique has been proven and tested. It is planned to employ the miniaturized test for further systematic investigations of damage mechanisms under high temperature fatigue on new single crystalline materials developed in the frame of the collaborative research centre SFB/Transregio 103 'From Atoms to Turbine Blades – a Scientific Approach for Developing the Next Generation of Single Crystal Superalloys' (<http://www.sfb-transregio103.de>).

### **Acknowledgement**

The authors acknowledge the financial support by the German Research Foundation (DFG) for project A3, SFB/Transregio 103.

- [1] Parsa A. et al. Advanced Scale Bridging Microstructure Analysis of Single Crystal Ni-Base Superalloys. *Adv. Eng. Mat.* 2015; 17 (2):216-230.
- [2] Schreuer J., Demtröder K. Temperature dependent elastic constants of heat treated CMSX-4. Ruhr-University Bochum, personal communication.
- [3] Hähner P., Affeldt E., Beck T., Klingelhöffer H., Loveday M., Rinaldi C., editors. Validated code-of-practice for strain-controlled thermomechanical fatigue testing. EUR 22281 EN-DG JRC, Luxembourg: Institute for Energy, Scientific and Technical Research series, ISBN 92-79-02216-4; 2006

### **6.4 Hydrogen embrittlement of pulse-plated nickel**

*E. D. Reese, W. Bestenbostel (AGI) and T. Sebold, G. Paronis (AD)*

The objective of the European funded project "Multiscale modelling of hydrogen embrittlement in crystalline materials (MultiHy)" is the development of multiscale models for hydrogen transport in complex microstructures, i.e. to develop a set of advanced modelling tools to assist in the evaluation of the susceptibility of metals to HE in realistic service conditions based on microstructural information. The validation and application of the models will be carried out by investigating the role of microstructure in industrial problems involving HE of advanced materials. For this, in-service conditions and the material manufacturing process have been reviewed. This information would form the basis for the development of numerical models for H-microstructure interactions and would also be correlated with experimental measurements in order to evaluate the H diffusion or trapping characteristics of certain microstructural features and defects. Thus, it was critical that the materials were characterised thoroughly and accurately.

In this study, three types of PP-Ni were investigated. Although the material consists of pure Ni, a modification of the microstructure and the mechanical properties can be achieved by variation of the plating parameters (e.g. current frequency, electrolyte). The microstructures which were generated were referred to as "common old (CO)", "common new (CN)" and "intermediate (IN)".

The results of the material characterisation may be summarised as follows:

- All PP-Ni materials were characterized by a dendritic grain structure. In the case of "common old" and "common new" the dendrites were clustered in elongated "columns", which were oriented parallel with the growth direction. These columns were larger for "common new" than for "common old". Columns were not discernible in the "intermediate" material.

- XRD measurements shows a slightly preferred orientation of the (200) and (111) planes in the growth direction for all materials. High angle grain boundaries (HAGBs) in “common old” and “common new” were uniformly distributed. In contrast, “intermediate” was characterised by an elevated proportion of HAGBs in the range 30-45°, as well as a lower proportion of low angle grain boundaries and a higher proportion of twins relative to the other materials.
- TEM analysis of the PP-Ni materials showed inclusions, which are possibly due to segregation of impurities. Also discovered through TEM analysis was the existence of nanocrystalline regions in the “intermediate” materials, which may correspond to the elevated proportion of grain boundaries with misorientations in the range 30-45°.
- Based on the microstructural analysis, it is not possible to explain the different susceptibilities of the PP-Ni materials to delayed H cracking in terms of differences in their microstructures.
- Fracture toughness tests confirmed the general tendency of the several materials for hydrogen embrittlement, revealing the progress in the material behaviour of the newly developed common new and intermediate material.

### **Acknowledgement**

This work is funded by the European Union under the Grant agreement number 263335.